

# RANDOMIZED COMPRESSION OF RANK-STRUCTURED MATRICES ACCELERATED WITH GRAPH COLORING \*

JAMES LEVITT<sup>†</sup> AND PER-GUNNAR MARTINSSON<sup>†</sup>

**Abstract.** A randomized algorithm for computing a data sparse representation of a given rank structured matrix  $\mathbf{A}$  (a.k.a. an  $\mathcal{H}$ -matrix) is presented. The algorithm draws on the randomized singular value decomposition (RSVD), and operates under the assumption that algorithms for rapidly applying  $\mathbf{A}$  and  $\mathbf{A}^*$  to vectors are available. The algorithm analyzes the hierarchical tree that defines the rank structure using graph coloring algorithms to generate a set of random test vectors. The matrix is then applied to the test vectors, and in a final step the matrix itself is reconstructed by the observed input-output pairs. The method presented is an evolution of the “peeling algorithm” of *L. Lin, J. Lu, and L. Ying, “Fast construction of hierarchical matrix representation from matrix–vector multiplication,” JCP, 230(10), 2011.* For the case of uniform trees, the new method substantially reduces the pre-factor of the original peeling algorithm. More significantly, the new technique leads to dramatic acceleration for many non-uniform trees since it constructs sample vectors that are optimized for a given tree. The algorithm is particularly effective for kernel matrices involving a set of points restricted to a lower dimensional object than the ambient space, such as a boundary integral equation defined on a surface in three dimensions.

**Key words.** randomized approximation of matrices, rank-structured matrices, HODLR matrix, hierarchically block separable matrix, hierarchically semiseparable matrix, fast direct solver

**AMS subject classifications.** 65N22, 65N38, 15A23, 15A52

**1. Introduction.** This work describes a set of efficient algorithms for handling large dense matrices that have *rank structure*. To simplify slightly, this means that an  $N \times N$  matrix can be tessellated into  $O(N)$  blocks in such a way that each block is either small or of low numerical rank, cf. Figures 3 and 1. This structure allows the matrix to be stored and applied to vectors efficiently, often with cost that scales linearly or close to linearly with  $N$ . Sometimes, it is also possible to compute an approximate inverse or LU factorization in linear or close to linear time. Matrices of this type have turned out to be ubiquitous in both engineering and data sciences, and have been the subject of much research in recent decades, going under names such as  $\mathcal{H}$ -matrices [3, 4, 12]; HODLR matrices [1, 18], Hierarchically Semi-Separable (HSS) matrices [6, 7, 25], Recursive Skeletonization [8, 14, 17, 23], and many more.

The specific problem we address is the following: Suppose that  $\mathbf{A}$  is an  $N \times N$  matrix that we know is rank-structured, but we do not have direct access to the low-rank factors that define the compressible off-diagonal blocks. Instead, we have access to fast algorithms that given tall thin matrices  $\mathbf{\Omega}, \mathbf{\Psi} \in \mathbb{R}^{N \times \ell}$ , evaluate the matrix-matrix products

$$\mathbf{Y} = \mathbf{A}\mathbf{\Omega}, \quad \text{and} \quad \mathbf{Z} = \mathbf{A}^*\mathbf{\Psi}.$$

The problem is then to construct two random matrices  $\mathbf{\Omega}$  and  $\mathbf{\Psi}$  for which  $\mathbf{A}$  can be recovered from the information in the set  $\{\mathbf{Y}, \mathbf{\Omega}, \mathbf{Z}, \mathbf{\Psi}\}$ . The algorithms described here solve the reconstruction problem using  $\ell \sim k \log(N)$  sample vectors, where  $k$  is an upper bound on the ranks of the off-diagonal blocks. The key novelty is the formulation of a graph coloring problem to analyze the cluster tree that defines the rank structure to build test matrices that are optimized for the specific problem under consideration.

\*Submitted to the editors DATE.

<sup>†</sup> Oden Institute for Computational Engineering and Sciences, University of Texas at Austin, Austin, TX (jlevitt@oden.utexas.edu, pgm@oden.utexas.edu).

The scheme presented has several important applications. First, it can be used to derive a rank-structured representation of any integral operator for which a fast matrix-vector multiplication algorithm, such as the Fast Multipole Method [10, 11], is available. Such a representation opens the door to a wider range of matrix operations such as LU factorization, matrix inversion, and sometimes even full spectral decompositions. Second, it can greatly simplify algebraic operations involving products of rank-structured matrices. For instance, the perhaps key application of rank-structured matrix algebra is the acceleration of sparse direct solvers, as the dense matrices that arise during LU factorization are often rank-structured. In the course of such a solver, a typical operation would be to form a Schur complement such as  $\mathbf{S}_{22} = \mathbf{A}_{21}\mathbf{A}_{11}^{-1}\mathbf{A}_{12}$  that would arise when the top left block  $\mathbf{A}_{11}$  is eliminated from a  $2 \times 2$  blocked matrix. If  $\mathbf{A}_{11}$  is rank-structured, then  $\mathbf{A}_{11}^{-1}$  can easily be applied to vectors via an LU factorization. If, additionally,  $\mathbf{A}_{12}$  and  $\mathbf{A}_{21}$  are either sparse or rank-structured, then  $\mathbf{S}_{22}$  can easily be applied to a vector. The technique described will then enable one to construct a data-sparse representation of  $\mathbf{S}_{22}$ . In contrast, to directly evaluate the product  $\mathbf{A}_{21}\mathbf{A}_{11}^{-1}\mathbf{A}_{12}$  is both onerous to code and slow to execute.

The method we describe is inspired by the “peeling algorithm” of [16], which to the best of our knowledge was the first true black box algorithm described in the literature. The method of [16] has formally the same sample complexity  $\ell \sim k \log(N)$  as our method, but involves substantially larger pre-factors. To be precise, [16] is targeted specifically for  $\mathcal{H}^1$ - and  $\mathcal{H}^2$ -matrices arising from the discretization of integral equations. Strong admissibility, and regular tree structures are used. In this environment, the method requires  $\ell \sim k 8^d \log(N)$  matrix-vector products involving  $\mathbf{A}$  and  $\mathbf{A}^*$ , where  $d$  is the dimension of space in which the underlying integral equation is defined. In contrast, the method presented here has complexity  $\ell \sim k 6^d \log(N)$  for fully populated uniform trees. For more general trees, the acceleration over the method of [16] is even more dramatic, since the adaptivity of our method enables it to exploit situations where the matrix arises from a set of points located on a lower dimensional geometric object. As an illustration, Section 5 reports on experiments involving a boundary integral equation defined on a 2D surface in three dimensional space, as well as examples in higher dimensions.

Another advantage of the techniques presented here is that they are not limited to the  $\mathcal{H}^1$  structure. To compress uniform  $\mathcal{H}^1$  and  $\mathcal{H}^2$  matrices, the presented algorithms obtain uniform basis matrices by sampling the interactions of a box with its entire interaction list collectively. This process results in higher quality samples while requiring fewer matrix-vector products compared to existing methods that approximate interactions between boxes separately and then apply a recompression step to obtain uniform basis matrices. More generally, the formulation of a graph coloring problem can be used to design test matrices for any tessellation (e.g., arising from some other geometric or algebraic admissibility condition).

*Remark 1.1* (Linear complexity schemes). A related class of algorithms for computing a rank-structured matrix by observing its action on certain structured random vectors was described in [19]. These techniques have true linear complexity (no logarithmic terms), and tend to be very fast in practice. However, they are not true black box algorithms, as they require the direct evaluation of a small number of entries of the matrix. In contrast, the method presented here is truly black box, like the methods of [16, 20].

The manuscript is structured as follows: Section 2 surveys some basic linear algebraic techniques that we rely on. Section 3 introduces our formalism for rank-

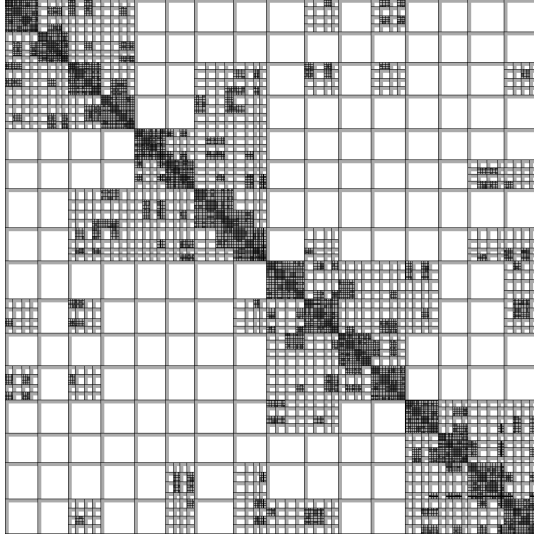


Fig. 1: An  $\mathcal{H}^1$  matrix for a quadtree over a uniform grid in the plane. Dense blocks are shown in dark gray, and low-rank blocks are represented with a white background and light gray rectangles representing the shapes of the low-rank factors.

structured matrices. Section 4 describes the new algorithm, and analyzes its asymptotic complexity. Section 5 describes numerical results.

## 2. Preliminaries.

**2.1. Notation.** Throughout the paper, we measure a vector  $\mathbf{x} \in \mathbb{R}^n$  by its Euclidean norm  $\|\mathbf{x}\| = (\sum_i |x_i|^2)^{\frac{1}{2}}$ . We measure a matrix  $\mathbf{A} \in \mathbb{R}^{m \times n}$  with the corresponding operator norm  $\|\mathbf{A}\| = \sup_{\|\mathbf{x}\|=1} \|\mathbf{A}\mathbf{x}\|$ , and in some cases with the Frobenius norm  $\|\mathbf{A}\|_{\text{Fro}} = (\sum_{i,j} |\mathbf{A}(i,j)|^2)^{1/2}$ . To denote submatrices, we use the notation of Golub and van Loan [9]: If  $\mathbf{A}$  is an  $m \times n$  matrix, and  $I = [i_1, i_2, \dots, i_k]$  and  $J = [j_1, j_2, \dots, j_l]$ , then  $\mathbf{A}(I, J)$  denotes the  $k \times l$  matrix

$$\mathbf{A}(I, J) = \begin{bmatrix} \mathbf{A}(i_1, j_1) & \mathbf{A}(i_1, j_2) & \dots & \mathbf{A}(i_1, j_l) \\ \mathbf{A}(i_2, j_1) & \mathbf{A}(i_2, j_2) & \dots & \mathbf{A}(i_2, j_l) \\ \vdots & \vdots & & \vdots \\ \mathbf{A}(i_k, j_1) & \mathbf{A}(i_k, j_2) & \dots & \mathbf{A}(i_k, j_l) \end{bmatrix}$$

We let  $\mathbf{A}(I, :)$  denote the column submatrix  $\mathbf{A}(I, [1, 2, \dots, n])$  and analogously let  $\mathbf{A}(:, J)$  denote a row submatrix of  $\mathbf{A}$ . We let  $\mathbf{A}^*$  denote the transpose of  $\mathbf{A}$ , and we say that matrix  $\mathbf{U}$  is *orthonormal* if its columns are orthonormal,  $\mathbf{U}^* \mathbf{U} = \mathbf{I}$ .

**2.2. The QR factorization.** The column-pivoted *QR factorization* of a matrix  $\mathbf{A}$  of size  $m \times n$  takes the form

$$(2.1) \quad \begin{array}{cc} \mathbf{A} & \mathbf{P} \\ m \times n & n \times n \end{array} = \begin{array}{cc} \mathbf{Q} & \mathbf{R} \\ m \times r & r \times n \end{array},$$

where  $r = \min(m, n)$ ,  $\mathbf{Q}$  is orthonormal,  $\mathbf{R}$  is upper-triangular, and  $\mathbf{P}$  is a permutation matrix. Representing the permutation matrix  $\mathbf{P}$  as the vector  $J \subset \mathbb{Z}_+^n$  of column

indices such that  $\mathbf{P} = \mathbf{I}(:, J)$ , the factorization (2.1) can be expressed as

$$\begin{array}{ccc} \mathbf{A}(:, J) & = & \mathbf{Q} \quad \mathbf{R}. \\ m \times n & & m \times r \quad r \times n \end{array}$$

For a matrix that is numerically low-rank, a rank- $k$  approximation of  $\mathbf{A}$  is given by a “partial QR factorization of  $\mathbf{A}$ ,”

$$\begin{array}{ccc} \mathbf{A}(:, J) & \approx & \mathbf{Q}_k \quad \mathbf{R}_k. \\ m \times n & & m \times k \quad k \times n \end{array}$$

**2.3. The singular value decomposition (SVD).** The singular value decomposition of a matrix  $\mathbf{A}$  of size  $m \times n$  takes the form

$$(2.2) \quad \begin{array}{ccc} \mathbf{A} & = & \mathbf{U} \quad \mathbf{\Sigma} \quad \mathbf{V}^*, \\ m \times n & & m \times r \quad r \times r \quad r \times n \end{array}$$

where  $r = \min(m, n)$ ,  $\mathbf{U}$  and  $\mathbf{V}$  are orthonormal matrices, and  $\mathbf{\Sigma}$  is a diagonal matrix with diagonal elements  $\{\sigma_j\}_{j=1}^r$  ordered such that  $\sigma_1 \geq \sigma_2 \geq \dots \geq \sigma_r \geq 0$ . The columns of  $\mathbf{U}$  and  $\mathbf{V}$ , denoted by  $\{\mathbf{u}_i\}_{i=1}^r$  and  $\{\mathbf{v}_i\}_{i=1}^r$ , are the left and right singular vectors of  $\mathbf{A}$ .

We let  $\mathbf{A}_k$  denote the rank- $k$  approximation obtained by truncating the SVD to its first  $k$  terms, so that  $\mathbf{A}_k = \sum_{j=1}^k \sigma_j \mathbf{u}_j \mathbf{v}_j^*$ . It then follows that

$$\|\mathbf{A} - \mathbf{A}_k\| = \sigma_{k+1} \quad \text{and that} \quad \|\mathbf{A} - \mathbf{A}_k\|_{\text{Fro}} = \left( \sum_{j=k+1}^{\min(m,n)} \sigma_j^2 \right)^{1/2}.$$

The Eckart–Young theorem asserts that  $\mathbf{A}_k$  achieves the smallest possible approximation error of  $\mathbf{A}$ , in both the operator and Frobenius norms, of any rank- $k$  matrix.

**2.4. Randomized compression.** In this section, we give a brief review of randomized low-rank approximation, following the presentation of [20]. Let  $\mathbf{A}$  be an  $m \times n$  matrix that can be accurately approximated by a matrix of rank  $k$ , and suppose we seek to determine a matrix  $\mathbf{Q}$  with orthonormal columns (as few as possible) such that  $\|\mathbf{A} - \mathbf{Q}\mathbf{Q}^*\mathbf{A}\|$  is small. In other words, we seek a matrix  $\mathbf{Q}$  whose columns form an approximate orthonormal basis (ON-basis) for the column space of  $\mathbf{A}$ . This task can efficiently be solved via the following randomized procedure:

1. Pick a small integer  $p$  representing how much “oversampling” is done. ( $p = 10$  is often good.)
2. Form an  $n \times (k + p)$  matrix  $\mathbf{G}$  whose entries are independent and identically distributed (i.i.d.) normalized Gaussian random numbers.
3. Form the “sample matrix”  $\mathbf{Y} = \mathbf{A}\mathbf{G}$  of size  $m \times (k + p)$ .
4. Construct an  $m \times (k + p)$  matrix  $\mathbf{Q}$  whose columns form an ON basis for the columns of  $\mathbf{Y}$ .

Note that each column of the sample matrix  $\mathbf{Y}$  is a random linear combination of the columns of  $\mathbf{A}$ . We would therefore expect the algorithm described to have a high probability of producing an accurate result when  $p$  is a large number. It is perhaps less obvious that this probability depends only on  $p$  (not on  $m$  or  $n$ , or any other properties of  $\mathbf{A}$ ) and that it approaches 1 extremely rapidly as  $p$  increases. In fact, one can show that the basis  $\mathbf{Q}$  determined by the scheme above satisfies

$$(2.3) \quad \|\mathbf{A} - \mathbf{Q}\mathbf{Q}^*\mathbf{A}\| \leq [1 + 11\sqrt{k+p} \cdot \sqrt{\min\{m, n\}}] \sigma_{k+1}$$

with probability at least  $1 - 6 \cdot p^{-p}$ ; see [13, sec. 1.5]. The error bound (2.3) indicates that the error produced by the randomized sampling procedure can be larger than the theoretically minimal error  $\sigma_{k+1}$  by a factor of  $1 + 11\sqrt{k+p} \cdot \sqrt{\min\{m,n\}}$ . This crude bound is typically very pessimistic, in particular for matrices whose singular values decay rapidly; cf. [13].

Now, suppose we would like to use the above sampling procedure to compute a low-rank factorization of the form

$$(2.4) \quad \begin{array}{ccccc} \mathbf{A} & = & \mathbf{U} & \mathbf{B} & \mathbf{V}, \\ m \times n & & m \times r & r \times r & r \times n \end{array}$$

where  $\mathbf{U}$  and  $\mathbf{V}$  have orthonormal columns and  $\mathbf{B}$  is a square matrix, not necessarily diagonal. We review two methods of completing this task using randomized sampling. The algorithm summarized in Algorithm 2.1 involves two randomized samples, one of  $\mathbf{A}$  and one of  $\mathbf{A}^*$ . It is based on so-called single-view algorithms for matrix compression [24, 22]. The second method [13], summarized in Algorithm 2.2, uses a randomized sample of  $\mathbf{A}$  to compute the column basis matrix  $\mathbf{U}$ , and then operates on the product  $\mathbf{A}^*\mathbf{U}$  to obtain  $\mathbf{B}$  and  $\mathbf{V}$ . We will use both methods in the algorithms described in section 4.

---

**Algorithm 2.1** Compress  $\mathbf{A} \approx \mathbf{UBV}^*$  via two randomized samples

---

Form  $n \times (k+p)$  Gaussian random matrix  $\mathbf{G}_1$  and  $m \times (k+p)$  Gaussian random matrix  $\mathbf{G}_2$ .

Multiply  $\mathbf{Y} = \mathbf{AG}_1$ .

Orthonormalize  $\mathbf{U} = \text{qr}(\mathbf{Y}, k)$ .

Multiply  $\mathbf{Z} = \mathbf{A}^*\mathbf{G}_2$ .

Orthonormalize  $\mathbf{V} = \text{qr}(\mathbf{Z}, k)$ .

Solve  $\mathbf{B} = (\mathbf{G}_2^*\mathbf{U})^\dagger \mathbf{G}_2^* \mathbf{AG}_1 (\mathbf{V}^*\mathbf{G}_1)^\dagger$ .

**return**  $\mathbf{U}, \mathbf{B}, \mathbf{V}$ .

---



---

**Algorithm 2.2** Compress  $\mathbf{A} \approx \mathbf{UBV}^*$  with one randomized and one deterministic sample

---

Form an  $n \times (k+p)$  Gaussian random matrix  $\mathbf{G}$ .

Multiply  $\mathbf{Y} = \mathbf{AG}$ .

Orthonormalize  $\mathbf{U} = \text{qr}(\mathbf{Y})$ .

Multiply  $\mathbf{W} = \mathbf{A}^*\mathbf{G}$ .

Orthonormalize  $[\mathbf{V}, \mathbf{B}^*] = \text{qr}(\mathbf{W})$ .

**return**  $\mathbf{U}, \mathbf{B}, \mathbf{V}$ .

---

**2.5. Functions for low-rank factorizations.** We introduce the following notation to denote calls to functions that return the results of QR factorizations and singular value decompositions. Function calls to evaluate the full factorizations are written as

$$[\mathbf{Q}, \mathbf{R}, J] = \text{qr}(\mathbf{A}), \quad [\mathbf{U}, \mathbf{\Sigma}, \mathbf{V}] = \text{svd}(\mathbf{A}).$$

Calls to evaluate the rank- $k$  truncated factorizations are written as

$$[\mathbf{Q}, \mathbf{R}, J] = \text{qr}(\mathbf{A}, k), \quad [\mathbf{U}, \mathbf{\Sigma}, \mathbf{V}] = \text{svd}(\mathbf{A}, k).$$

We write

$$[\mathbf{Q}, \mathbf{R}] = \text{qr}(\mathbf{A}), \quad \mathbf{Q} = \text{qr}(\mathbf{A})$$

to compute an unpivoted QR factorization and to compute just the factor  $\mathbf{Q}$  via the Gram-Schmidt process, respectively.

**2.6. The degree of saturation graph coloring algorithm.** A vertex coloring of graph is an assignment of a color to each vertex in such a way that no pair of adjacent vertices shares the same color. The problem of finding a vertex coloring with the minimum number of colors is NP-hard, but there exist a number of algorithms for efficiently coloring graphs, though they may produce colorings with more than the minimum number of colors.

Greedy graph coloring algorithms process the vertices in sequence, at each iteration assigning to one vertex the first available color that hasn't already been assigned to one of its neighbors. In the *degree of saturation* (DSatur) algorithm [5], the choice of which vertex to color at each step is made by selecting from the remaining uncolored vertices the one whose neighbors have the greatest number of distinct colors (the so-called degree of saturation). The procedure is summarized in [Algorithm 2.3](#).

---

**Algorithm 2.3** Greedy graph coloring with DSatur

---

Initialize priority queue  $q$  of vertices keyed by degree of saturation (initially all zero)

Initialize for each vertex a set of invalid colors (initially all empty)

**while**  $q$  is not empty **do**

Pop from  $q$  the vertex  $v$  with highest degree of saturation  $\triangleright \mathcal{O}(\log |V|)$

Assign a color to  $v$ , creating a new one if necessary  $\triangleright \mathcal{O}(\deg(G))$

**for** each vertex  $w$  adjacent to  $v$  **do**

Add the color of  $v$  to the set of invalid colors for  $w$   $\triangleright \mathcal{O}(1)$

Update the priority of  $w$  within  $q$   $\triangleright \mathcal{O}(\log |V|)$

---

While the asymptotic complexity of DSatur is often described as quadratic in the number of vertices, the algorithm can be implemented with quasilinear complexity, assuming the degree of the graph is bounded. Summing the costs listed in [Algorithm 2.3](#), we find that the asymptotic complexity is

$$(2.5) \quad T_{\text{color}} \sim \deg(G)|V| \log |V|,$$

where  $\deg(G)$  denotes the degree of the graph. for the step of assigning a color to vertex  $v$ , we note that a greedy coloring algorithm uses no more than  $\deg(G) + 1$  colors in the worst case, so checking the existing colors for whether they belong to the set of invalid colors for  $v$  requires  $\mathcal{O}(\deg(G))$  operations.

**3. Rank-structured matrices.** Let  $X = [0, 1]^d$  be a  $d$ -dimensional hypercube. We introduce a tree of boxes, each level of which represents a partition of  $X$  into smaller boxes. Level 0 only contains a single node, which corresponds to  $X$ . The boxes belonging to level  $l + 1$  are obtained by bisecting each of the boxes in level  $l$  along each dimension to form  $2^d$  smaller boxes. The  $2^d$  boxes in level  $l + 1$  obtained by splitting a box in level  $l$  are designated as the children of that box, giving rise to the tree structure. Boxes that do not contain any points are omitted from the tree, so the branching factor of the tree may be less than  $2^d$ , depending on the distribution of points. The splitting procedure is applied recursively to boxes that contain more than  $m$  points, where  $m$  is a prespecified maximum number of points to allow in a leaf box.

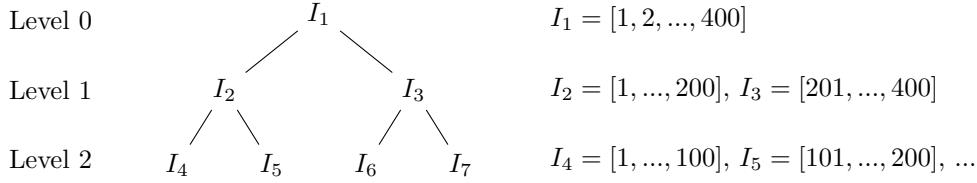


Fig. 2: A binary tree structure, where the levels of the tree represent successively refined partitions of the index vector  $[1, \dots, 400]$ .

We let  $L$  denote the depth of the tree, and assume that the points are distributed throughout the domain in such a way that  $L \sim \log N$ .

Two boxes that belong to the same level and have overlapping boundaries are said to be *neighbors*. The neighbors of box  $\tau$ , of which there are up to  $3^d$  (including  $\tau$  itself), are stored in the *neighbor list* of  $\tau$ , denoted by  $\mathcal{L}_\tau^{\text{nei}}$ . The *interaction list* of  $\tau$ , denoted by  $\mathcal{L}_\tau^{\text{int}}$  contains the children of neighbors of the parent of  $\tau$ , excluding those that are neighbors of  $\tau$ . The interaction list of a box contains up to  $6^d - 3^d$  boxes.

Let  $\{x_i\}_{i=1}^N \subset X$  be a set of points within the domain, and let  $\mathbf{A}$  be an  $N$ -by- $N$  matrix where

$$\mathbf{A}(i, j) = \mathcal{K}(x_i, x_j) \quad 1 \leq i \leq N, 1 \leq j \leq N,$$

for some kernel function  $\mathcal{K}$ . That is, the  $(i, j)$  entry of  $\mathbf{A}$  represents an interaction between points  $x_i, x_j$  as defined by  $\mathcal{K}$ . For each box  $\tau$ , we assign a list of indices of the points contained by the box,  $I_\tau = \{i : x_i \in \tau\}$ . Figure 2 shows an example tree structure and index lists.

Matrix  $\mathbf{A}$  is said to have  $\mathcal{H}^1$  structure if block  $\mathbf{A}(I_\alpha, I_\beta)$  is numerically low-rank, for all pairs of boxes  $\alpha, \beta$  belonging to the interaction lists of one another. Such blocks, and the corresponding pairs of boxes, are said to be *admissible*. Figure 3 shows a tessellation of a matrix consisting of the admissible blocks as well as a number of *inadmissible* blocks of interactions between neighboring boxes in level  $L$ , which are not necessarily low-rank. Constructing a compressed representation of an  $\mathcal{H}^1$  matrix consists of finding low rank approximations

$$\mathbf{A}(I_\alpha, I_\beta) \approx \mathbf{U}_{\alpha, \beta} \mathbf{B}_{\alpha, \beta} \mathbf{V}_{\alpha, \beta}$$

for each admissible pair  $(\alpha, \beta)$  and storing the inadmissible blocks corresponding to neighbor interactions of boxes in level  $L$ .

An  $\mathcal{H}^1$  matrix  $\mathbf{A}$  is said to have uniform  $\mathcal{H}^1$  structure if it further satisfies the condition that there exist low-rank basis matrices  $\mathbf{U}_\alpha$  spanning  $\mathbf{A}(I_\alpha, \cup_{\beta \in \mathcal{L}_\alpha^{\text{int}}} I_\beta)$  and  $\mathbf{V}_\alpha$  spanning  $\mathbf{A}(\cup_{\beta \in \mathcal{L}_\alpha^{\text{int}}} I_\beta, I_\alpha)$  for each box  $\alpha$ . Constructing a compressed representation of a uniform  $\mathcal{H}^1$  matrix consists of finding the matrices  $\mathbf{U}_\alpha, \mathbf{V}_\alpha$  for each box  $\alpha$  and the matrices  $\mathbf{B}_{\alpha, \beta}$  such that

$$\mathbf{A}(I_\alpha, I_\beta) \approx \mathbf{U}_\alpha \mathbf{B}_{\alpha, \beta} \mathbf{V}_\beta$$

for each admissible pair  $(\alpha, \beta)$  and storing the inadmissible blocks corresponding to neighbor interactions of boxes in level  $L$ .

A uniform  $\mathcal{H}^1$  matrix  $\mathbf{A}$  is said to have  $\mathcal{H}^2$  structure if there exist low-rank basis matrices  $\mathbf{U}_\alpha$  spanning  $\mathbf{A}(I_\alpha, (\cup_{\beta \in \mathcal{L}_\alpha^{\text{nei}}} I_\beta)^c)$  and  $\mathbf{V}_\alpha$  spanning  $\mathbf{A}((\cup_{\beta \in \mathcal{L}_\alpha^{\text{nei}}} I_\beta)^c, I_\alpha)$  for

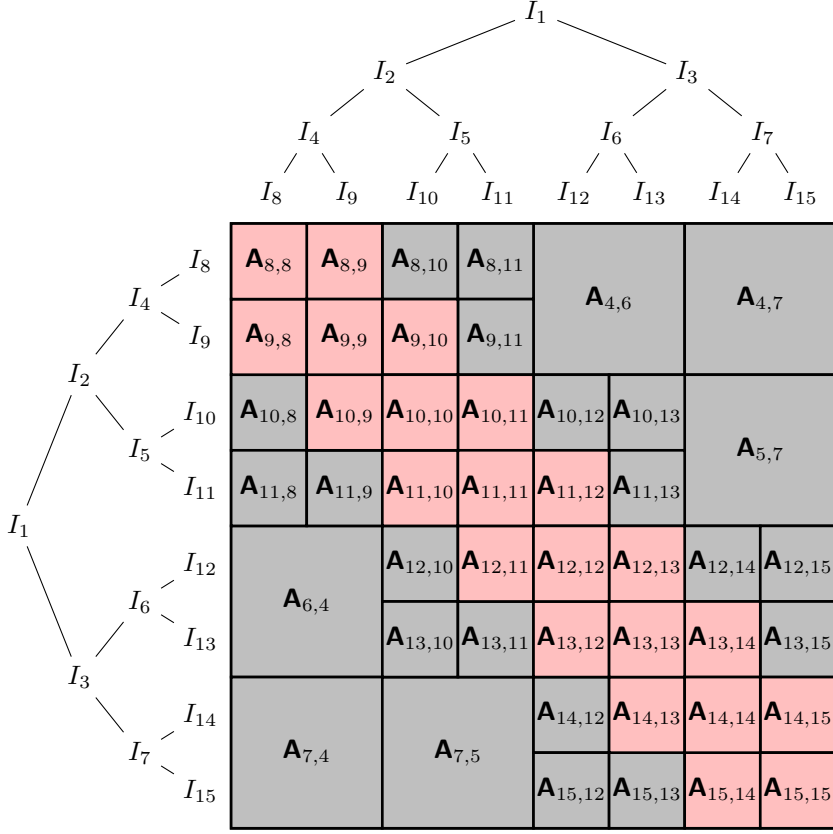


Fig. 3: An  $\mathcal{H}^1$  matrix with depth 3 based on a grid over  $[0, 1]$ . Admissible blocks are shown in gray, and inadmissible blocks are shown in pink.

each box  $\alpha$ . Then the basis matrices of a non-leaf box can be expressed in terms of the basis matrices of its children. For example, if  $\tau$  is a box with children  $\alpha, \beta$ , then

$$(3.1) \quad \mathbf{u}_\tau = \begin{bmatrix} \mathbf{u}_\alpha & \mathbf{0} \\ \mathbf{0} & \mathbf{u}_\beta \end{bmatrix} \mathbf{U}_\tau,$$

where  $\mathbf{u}_\gamma$  is the “long” column basis matrix of size  $|\gamma| \times k$  associated with  $\gamma \in \{\tau, \alpha, \beta\}$ , and  $\mathbf{U}_\tau$  is a “short” basis matrix of size  $2k \times k$ . Analogous relationships must hold for row basis matrices  $\mathbf{v}_\tau, \mathbf{v}_\alpha, \mathbf{v}_\beta$ . Using such nested basis matrices eliminates the need to explicitly store  $\mathbf{u}_\tau$  since it is fully specified by  $\mathbf{u}_\alpha, \mathbf{u}_\beta$  and  $\mathbf{U}_\tau$ . Likewise, if  $\alpha$  or  $\beta$  have children of their own, then their basis matrices will be expressed in terms of their own small basis matrices and the basis matrices of their children.

#### 4. Compressing rank-structured matrices with graph coloring.

**4.1.  $\mathcal{H}^1$  matrix compression.** In this section, we present the process of constructing an  $\mathcal{H}^1$  representation of a matrix by applying [Algorithm 2.1](#) to compute low-rank approximations of the admissible blocks of levels  $2, \dots, L$  and then extracting the inadmissible blocks of level  $L$ . We apply  $A$  and  $A^*$  to a set of carefully constructed test matrices, and from those products we extract randomized samples



of each admissible block. We demonstrate the techniques on a matrix shown in [Figure 3](#), which is based on points in one dimension, but the algorithm generalizes in a straightforward way to points higher dimensions.

**4.1.1. Compressing level 2.** We construct the compressed representation by processing levels of the tree in sequence from the coarsest level to the finest. There are no admissible blocks associated with levels 0 and 1, so we begin by computing low-rank approximations of the 6 admissible blocks associated with level 2 of the tree. To that end, we define four test matrices of size  $N \times r$

$$\Omega_1 = \begin{bmatrix} \mathbf{G}_4 \\ \mathbf{0} \\ \mathbf{0} \\ \mathbf{0} \end{bmatrix}, \quad \Omega_2 = \begin{bmatrix} \mathbf{0} \\ \mathbf{G}_5 \\ \mathbf{0} \\ \mathbf{0} \end{bmatrix}, \quad \Omega_3 = \begin{bmatrix} \mathbf{0} \\ \mathbf{0} \\ \mathbf{G}_6 \\ \mathbf{0} \end{bmatrix}, \quad \Omega_4 = \begin{bmatrix} \mathbf{0} \\ \mathbf{0} \\ \mathbf{0} \\ \mathbf{G}_7 \end{bmatrix},$$

where  $\mathbf{G}_4, \mathbf{G}_5, \mathbf{G}_6, \mathbf{G}_7$  are random matrices of size  $N/4 \times r$  whose entries are drawn from the standard normal distribution. We invoke the black-box matrix-vector product routine to evaluate the products  $\mathbf{Y}_i = \mathbf{A}\Omega_i, i \in \{1, 2, 3, 4\}$ , with the following structures. Contained within these products are randomized samples of each admissible block of level 2.

$$(4.1) \quad \begin{aligned} \mathbf{Y}_1 = \mathbf{A}\Omega_1 &= \begin{bmatrix} * \\ * \\ \mathbf{A}_{6,4}\mathbf{G}_4 \\ \mathbf{A}_{7,4}\mathbf{G}_4 \end{bmatrix}, & \mathbf{Y}_2 = \mathbf{A}\Omega_2 &= \begin{bmatrix} * \\ * \\ * \\ \mathbf{A}_{7,5}\mathbf{G}_5 \end{bmatrix} \\ \mathbf{Y}_3 = \mathbf{A}\Omega_3 &= \begin{bmatrix} \mathbf{A}_{4,6}\mathbf{G}_6 \\ * \\ * \\ * \end{bmatrix}, & \mathbf{Y}_4 = \mathbf{A}\Omega_4 &= \begin{bmatrix} \mathbf{A}_{4,7}\mathbf{G}_7 \\ \mathbf{A}_{5,7}\mathbf{G}_7 \\ * \\ * \end{bmatrix} \end{aligned}$$

We then obtain a basis matrix for the column space of each admissible block by orthonormalizing the relevant block of one of the sample matrices.

$$(4.2) \quad \begin{aligned} \mathcal{U}_{4,6} &= \text{qr}(\mathbf{Y}_3(I_4, :)) \\ \mathcal{U}_{4,7} &= \text{qr}(\mathbf{Y}_4(I_4, :)) \\ \mathcal{U}_{5,7} &= \text{qr}(\mathbf{Y}_4(I_5, :)) \\ \mathcal{U}_{6,4} &= \text{qr}(\mathbf{Y}_1(I_6, :)) \\ \mathcal{U}_{7,4} &= \text{qr}(\mathbf{Y}_1(I_7, :)) \\ \mathcal{U}_{7,5} &= \text{qr}(\mathbf{Y}_2(I_7, :)) \end{aligned}$$

To find a basis matrix for the row space of each admissible block, we follow a similar process using  $\mathbf{A}^*$  in place of  $\mathbf{A}$ . That is, we compute another set of sample matrices  $\mathbf{Z}_i = \mathbf{A}^*\boldsymbol{\Psi}_i, i \in \{1, 2, 3, 4\}$ , from which we orthonormalize the relevant blocks to obtain row bases  $\mathcal{V}_{\alpha,\beta}$  for each admissible pair  $(\alpha, \beta)$ .

Finally, we solve for the matrices  $\mathbf{B}_{\alpha,\beta}$  as follows. Note that the products  $\mathbf{A}_{\alpha,\beta}\mathbf{G}_\beta$  have already been obtained from the samples in (4.1).

$$(4.3) \quad \mathbf{B}_{\alpha,\beta} = (\mathbf{G}_\alpha \mathcal{U}_\alpha)^\dagger \mathbf{G}_\alpha \mathbf{A}_{\alpha,\beta} \mathbf{G}_\beta (\mathcal{V}_\beta \mathbf{G}_\beta)^\dagger \quad \text{for each admissible pair } (\alpha, \beta)$$

**4.1.2. Compressing levels 3, ...,  $L$ .** After we have obtained low-rank approximations of the blocks associated with level 2 of the tree, we proceed to level 3. One approach would be to extend the procedure for level 2 by using one test matrix corresponding to each box, for a total of eight test matrices. That approach would grow to be prohibitively expensive for finer levels of the tree as the number of matrix-vector products required would grow proportionately with the number of boxes. Instead, we present a more efficient procedure, which requires a number of matrix-vector products that is bounded across all levels.

Following [20], we define the level- $l$  truncated matrix  $\mathbf{A}^{(l)}$  to be the matrix obtained by replacing with zeros every block of  $\mathbf{A}$  corresponding to levels finer than level  $l$ . Note that a matrix-vector product involving  $\mathbf{A}^{(l)}$  can be computed inexpensively using the low-rank approximations already computed when processing levels  $2, \dots, l-1$ . The structures of the level-2 truncated matrix and the difference  $\mathbf{A} - \mathbf{A}^{(2)}$  are shown below.

$$\mathbf{A}^{(2)} = \begin{array}{|c|c|c|c|} \hline & & \mathbf{A}_{4,6} & \mathbf{A}_{4,7} \\ \hline & & & \mathbf{A}_{5,7} \\ \hline & \mathbf{0} & & \\ \hline \mathbf{A}_{6,4} & & & \\ \hline \mathbf{A}_{7,4} & \mathbf{A}_{7,5} & & \\ \hline \end{array}, \quad \mathbf{A} - \mathbf{A}^{(2)} = \begin{array}{|c|c|c|c|c|c|} \hline & & & & \mathbf{0} & \mathbf{0} \\ \hline & & & & \mathbf{0} & \mathbf{0} \\ \hline & & & & & \mathbf{0} \\ \hline & & & & & \\ \hline \mathbf{0} & & & & & \\ \hline \mathbf{0} & \mathbf{0} & & & & \\ \hline \end{array}$$

We will sample the admissible blocks of level 3 by applying  $\mathbf{A} - \mathbf{A}^{(2)}$  to a set of test matrices subject to certain conditions on their sparsity structure. For example, to isolate a sample of  $\mathbf{A}_{8,10}$  (see Figure 3), we must avoid unwanted contributions from  $\mathbf{A}_{8,8}, \mathbf{A}_{8,9}, \mathbf{A}_{8,11}$ , so we multiply  $\mathbf{A} - \mathbf{A}^{(2)}$  with a test matrix whose rows indexed by  $I_8, I_9, I_{11}$  are all zeros and whose rows indexed by  $I_{10}$  are filled with random values drawn from the standard normal distribution. The contents of the other rows are irrelevant for the purpose of sampling  $\mathbf{A}_{8,10}$  since they will be multiplied with zeros in  $\mathbf{A} - \mathbf{A}^{(2)}$ . More generally, to sample some admissible block  $\mathbf{A}_{\alpha,\beta}$  of level 3, we require a test matrix  $\mathbf{\Omega}$  that satisfies the following *sampling constraints*.

$$(4.4) \quad \begin{aligned} \mathbf{\Omega}(I_\beta, \cdot) &= \mathbf{G}_\beta \\ \mathbf{\Omega}(I_\gamma, \cdot) &= \mathbf{0} \quad \text{for all } \gamma \in \mathcal{L}_\alpha^{\text{nei}} \cup \mathcal{L}_\alpha^{\text{int}} \setminus \{\beta\} \end{aligned}$$

where  $\mathbf{G}_\beta$  is a random matrix of size  $|I_\beta|$ -by- $r$ . If test matrix  $\mathbf{\Omega}$  satisfies those sampling constraints, then the rows of the product  $\mathbf{A}\mathbf{\Omega} - \mathbf{A}^{(2)}\mathbf{\Omega}$  indexed by  $I_\alpha$  will contain a randomized sample of the column space of  $\mathbf{A}_{\alpha,\beta}$ .

To sample all of the admissible blocks, we require a set of test matrices  $\{\mathbf{\Omega}_i\}$  such that for every admissible pair  $(\alpha, \beta)$ , there is a test matrix within the set that satisfies the constraints (4.4) associated with that pair. Moreover, we would like that set to be as small as possible to minimize cost.

In order to minimize the number of test matrices, we aim to form a small number of groups of compatible sampling constraints. We say that two sets of sampling constraints are *compatible* if it is possible to form a test matrix  $\mathbf{\Omega}$  that satisfies both

sets of constraints. We then define a *constraint incompatibility graph*, which represents compatibility relationships between pairs of constraint sets. The graph corresponding to the 18 admissible blocks belonging to level 3 is depicted in Figure 4.

**DEFINITION 4.1** (Constraint incompatibility graph). *The constraint incompatibility graph for level  $l$  of the tree is the graph in which each vertex corresponds to a distinct constraint set (4.4), and pairs of vertices are connected by an edge if their corresponding constraint sets are incompatible.*

We then compute a vertex coloring of the constraint incompatibility graph using the DSatur algorithm (Algorithm 2.3). For a valid coloring of the graph, each subset of vertices sharing the same color represents a mutually compatible collection of sampling constraints. Then for each color, we can define one test matrix that satisfies all of the sampling constraints associated with the vertices of that color. The coloring shown in Figure 4 yields test matrices with the following structures.

$$(4.5) \quad [\Omega_1 \quad \Omega_2 \quad \Omega_3 \quad \Omega_4 \quad \Omega_5 \quad \Omega_6] = \begin{bmatrix} \mathbf{G}_8 & \mathbf{0} & \mathbf{0} & \mathbf{0} & \mathbf{0} & \mathbf{0} \\ \mathbf{0} & \mathbf{G}_9 & \mathbf{0} & \mathbf{0} & \mathbf{0} & \mathbf{0} \\ \mathbf{0} & \mathbf{0} & \mathbf{G}_{10} & \mathbf{0} & \mathbf{0} & \mathbf{0} \\ \mathbf{0} & \mathbf{0} & \mathbf{0} & \mathbf{G}_{11} & \mathbf{0} & \mathbf{0} \\ \mathbf{0} & \mathbf{0} & \mathbf{0} & \mathbf{0} & \mathbf{G}_{12} & \mathbf{0} \\ \mathbf{0} & \mathbf{0} & \mathbf{0} & \mathbf{0} & \mathbf{0} & \mathbf{G}_{13} \\ \mathbf{G}_{14} & \mathbf{0} & \mathbf{0} & \mathbf{0} & \mathbf{0} & \mathbf{0} \\ \mathbf{0} & \mathbf{G}_{15} & \mathbf{0} & \mathbf{0} & \mathbf{0} & \mathbf{0} \end{bmatrix}$$

As in subsection 4.1.1, we evaluate the samples  $\mathbf{Y}_i = \mathbf{A}\Omega_i - \mathbf{A}^{(2)}\Omega_i$  and orthonormalize the relevant blocks to obtain orthonormal bases  $\mathbf{U}_{\alpha,\beta}$  of the column spaces of the admissible blocks. A similar process yields orthonormal bases  $\mathbf{V}_{\alpha,\beta}$  of the row spaces. Finally, we solve for  $\mathbf{B}_{\alpha,\beta}$  again using (4.3).

**4.1.3. Extracting inadmissible blocks of the leaf level.** Once we have computed low-rank approximations of the admissible blocks for every level, we finally extract the the inadmissible blocks of the leaf level. Since the inadmissible blocks are not necessarily low-rank, they cannot be recovered from a small number of randomized samples. Instead, we use test matrices that will multiply the inadmissible blocks with appropriately sized identity matrices. Also, at this point we already have low-rank approximations of the admissible blocks belonging to level  $L$ , so the test matrices only need to avoid contributions from other inadmissible blocks, resulting in fewer constraints than (4.4). To extract inadmissible block  $\mathbf{A}_{\alpha,\beta}$  of level  $L$ , we require a test matrix  $\Omega$  that satisfies the following sampling constraints.

$$\begin{aligned} \Omega(I_\beta, :) &= \mathbf{I} \\ \Omega(I_\gamma, :) &= \mathbf{0} \quad \text{for all } \gamma \in \mathcal{L}_\alpha^{\text{nei}} \setminus \{\beta\} \end{aligned}$$

If test matrix  $\Omega$  satisfies these constraints, then the rows of the product  $\mathbf{A}\Omega - \mathbf{A}^{(2)}\Omega$  indexed by  $I_\alpha$  will contain  $\mathbf{A}_{\alpha,\beta}$ . The graph corresponding to the 22 inadmissible blocks belonging to level 3 is depicted in Figure 5, and its coloring produces test matrices with the following structures. The entire process of compressing an  $\mathcal{H}^1$  matrix is summarized in Algorithm 4.1.

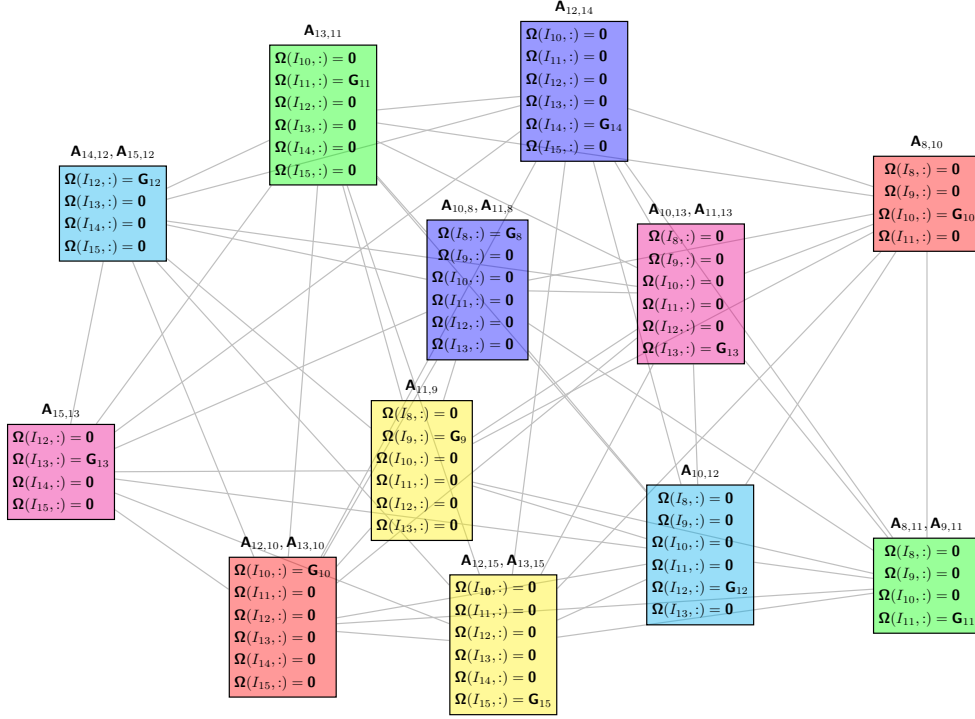
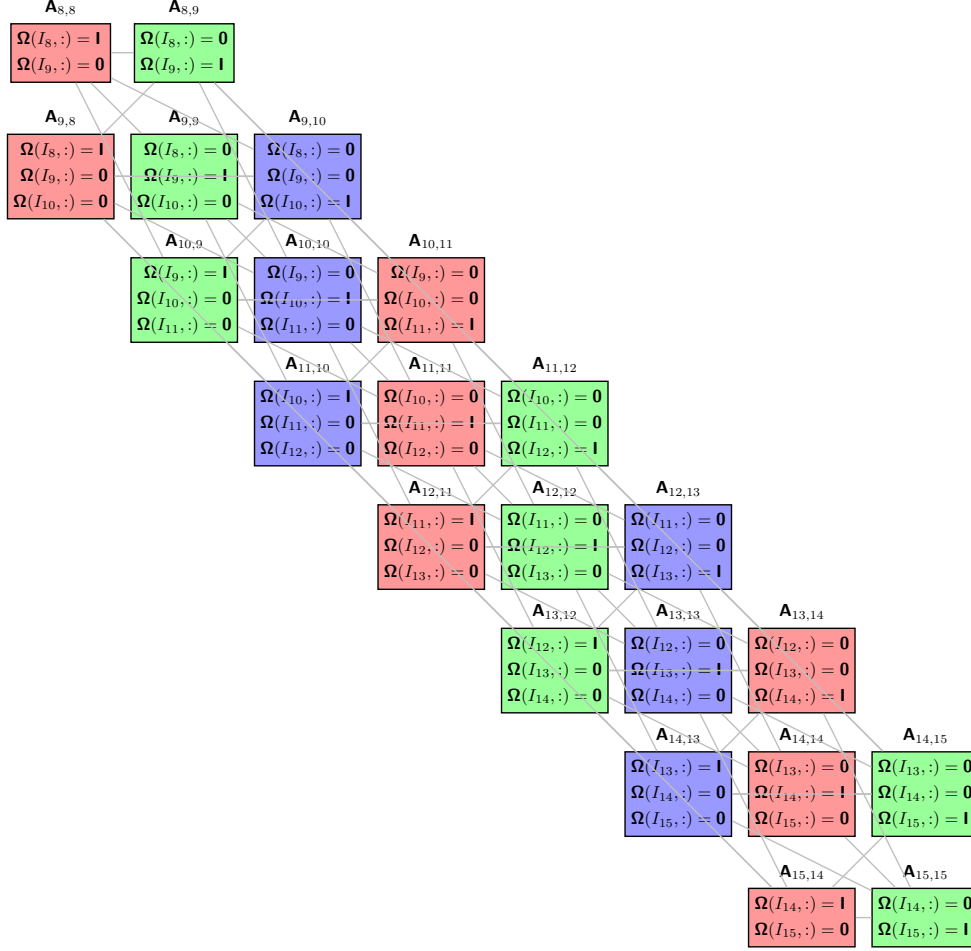


Fig. 4: The constraint incompatibility graph corresponding to the 18 admissible blocks belonging to level 3 of the matrix shown in Figure 3. Each vertex corresponds to a distinct set of sampling constraints (4.4). Edges connect pairs of vertices that are incompatible. The number of vertices is less than the number of admissible blocks since some admissible blocks share the same set of sampling constraints.

$$[\Omega_1 \quad \Omega_2 \quad \Omega_3] = \begin{bmatrix} \mathbf{G}_8 & \mathbf{0} & \mathbf{0} \\ \mathbf{0} & \mathbf{G}_9 & \mathbf{0} \\ \mathbf{0} & \mathbf{0} & \mathbf{G}_{10} \\ \mathbf{G}_{11} & \mathbf{0} & \mathbf{0} \\ \mathbf{0} & \mathbf{G}_{12} & \mathbf{0} \\ \mathbf{0} & \mathbf{0} & \mathbf{G}_{13} \\ \mathbf{G}_{14} & \mathbf{0} & \mathbf{0} \\ \mathbf{0} & \mathbf{G}_{15} & \mathbf{0} \end{bmatrix}$$

**4.1.4. General patterns in the test matrices for  $\mathcal{H}^1$  compression.** In this section, we describe sets of test matrices that are sufficient for compressing any  $\mathcal{H}^1$  matrix based on points in arbitrary dimensions. Though sufficient, these sets of test matrices are not necessarily the smallest possible, and the proposed method of constructing problem-specific test matrices via graph coloring often yields a smaller set of test matrices, resulting in fewer matrix-vector products. The test matrices described in this section establish an upper bound on the number of matrix-vector products that improves on the number given in [16], and they also imply a bound

Fig. 5: Incompatibility graph for inadmissible blocks belonging to level  $L$ .

on the chromatic number of the graph, which appears in the estimate of asymptotic complexity.

*A general set of test matrices for sampling admissible blocks.* The structures of the test matrices derived in subsections 4.1.2 and 4.1.3 exhibit patterns that generalize to finer and higher-dimensional grids. The sampling constraints (4.4) for admissible block  $\mathbf{A}_{\alpha,\beta}$  specify that the rows of the test matrix corresponding to  $\beta$  must be filled with random values, and the rows of the test matrix corresponding to the other boxes in  $\mathcal{L}_\alpha^{\text{nei}} \cup \mathcal{L}_\alpha^{\text{int}}$  must be filled with zeros. For a 1-dimensional problem, the indices corresponding to  $\mathcal{L}_\alpha^{\text{nei}} \cup \mathcal{L}_\alpha^{\text{int}}$  form 6 contiguous blocks of the test matrix. Accordingly, each of the test matrices defined in (4.1) has every sixth block filled with random values and the other blocks filled with zeros, a pattern that generalizes to an arbitrarily fine grid in one dimension.

To describe a general set of test matrices for a problem in 2 dimensions, we partition the domain into tiles, each of which covers  $6 \times 6$  boxes. We define 36 test matrices, each activating a set of boxes that share the same position within their

---

**Algorithm 4.1** Randomized compression of an  $\mathcal{H}^1$  matrix
 

---

**for** level  $l \in [2, \dots, L]$  **do**  
   Compute randomized samples of  $\mathbf{A} - \mathbf{A}^{(l)}$   
   Construct structured random test matrices  $\{\boldsymbol{\Omega}_i\}$  of size  $N \times (k + p)$  as in [subsection 4.1.2](#) or [subsection 4.1.4](#)  
   **for all**  $\boldsymbol{\Omega}_i$  **do**  
     Multiply  $\mathbf{Y}_i = \mathbf{A}\boldsymbol{\Omega}_i - \mathbf{A}^{(l)}\boldsymbol{\Omega}_i$   
  
     Compute orthonormal basis matrices  $\mathcal{U}_{\alpha,\beta}$   
     **for all** interacting pairs  $\alpha, \beta$  in level  $l$  **do**  
       Identify  $\mathbf{Y}_i$  that contains a sample of  $\mathbf{A}_{\alpha,\beta}$  in  $\mathbf{Y}_i(I_\alpha, :)$   
       Orthonormalize  $\mathcal{U}_{\alpha,\beta} = \text{qr}(\mathbf{Y}_i(I_\alpha, :), k)$   
  
     Compute randomized samples of  $\mathbf{A}^* - \mathbf{A}^{(l)*}$   
     Construct structured random test matrices  $\{\boldsymbol{\Psi}_i\}$  of size  $N \times (k + p)$  as in [subsection 4.1.2](#) or [subsection 4.1.4](#) (if the rank structure of  $\mathbf{A}$  is symmetric, then the test matrices  $\{\boldsymbol{\Omega}_i\}$  can be reused)  
     **for all**  $\boldsymbol{\Psi}_i$  **do**  
       Multiply  $\mathbf{Z}_i = \mathbf{A}^*\boldsymbol{\Psi}_i - \mathbf{A}^{(l)*}\boldsymbol{\Psi}_i$   
  
     Compute orthonormal basis matrices  $\mathcal{V}_{\alpha,\beta}$   
     **for all** interacting pairs  $\alpha, \beta$  in level  $l$  **do**  
       Identify  $\mathbf{Z}_i$  that contains a sample of  $\mathbf{A}_{\alpha,\beta}^*$  in  $\mathbf{Z}_i(I_\beta, :)$   
       Orthonormalize  $\mathcal{V}_{\alpha,\beta} = \text{qr}(\mathbf{Z}_i(I_\beta, :), k)$   
  
     Solve for  $\mathbf{B}$   
     **for all** interacting pairs  $\alpha, \beta$  in level  $l$  **do**  
        $\mathbf{B}_{\alpha,\beta} = (\mathbf{G}_\alpha \mathcal{U}_\alpha)^\dagger \mathbf{G}_\alpha \mathbf{A}_{\alpha,\beta} \mathbf{G}_\beta (\mathcal{V}_\beta \mathbf{G}_\beta)^\dagger$   
  
   Extract the inadmissible blocks of level  $L$   
   Construct structured random test matrices  $\{\boldsymbol{\Omega}_i\}$  of size  $N \times m$  as in [subsection 4.1.3](#) or [subsection 4.1.4](#)  
   **for all**  $\boldsymbol{\Omega}_i$  **do**  
     Multiply  $\mathbf{Y}_i = \mathbf{A}\boldsymbol{\Omega}_i - \mathbf{A}^{(L)}\boldsymbol{\Omega}_i$   
   **for all** neighbor pairs  $\alpha, \beta$  in level  $L$  **do**  
     Identify  $\mathbf{Y}_i$  that contains  $\mathbf{A}_{\alpha,\beta}$   
     Extract the block  $\mathbf{A}_{\alpha,\beta}$  from  $\mathbf{Y}_i(I_\alpha, :)$

---

respective tiles. The set of boxes activated by one of the test matrices is shown in [Figure 6](#). The sampling constraints in (4.4) apply to  $\mathcal{L}_\alpha^{\text{nei}} \cup \mathcal{L}_\alpha^{\text{int}}$ , which form a square of  $6 \times 6$  boxes, and they specify that exactly one of those boxes must be activated. Therefore, those constraints will be satisfied by one of the 36 test matrices. By a similar argument, this pattern generalizes to higher-dimensional problems, requiring at most  $6^d$  test matrices to sample one level of admissible blocks for a problem in  $d$  dimensions. Furthermore, since these test matrices satisfy (4.4), they must correspond to a valid coloring of the graph described in [subsection 4.1.2](#), bounding the chromatic

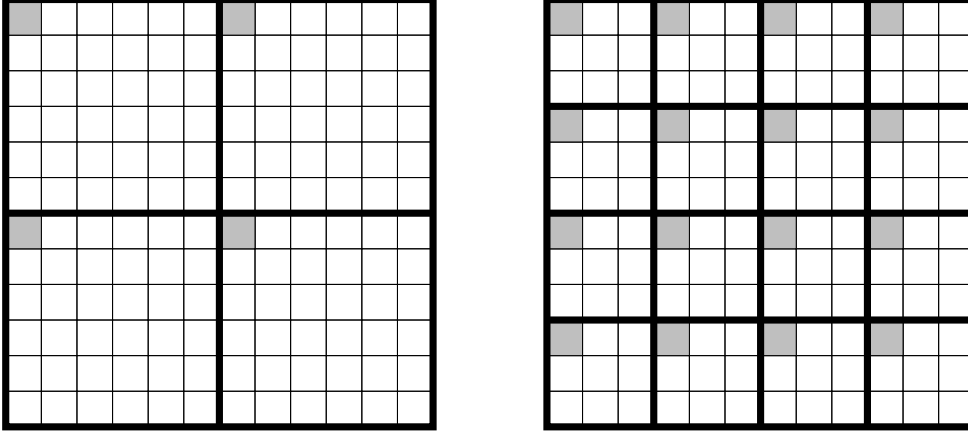


Fig. 6: Patterns representing a test matrix for sampling admissible blocks (left) and a test matrix for sampling inadmissible blocks (right) for a problem in 2 dimensions. Blocks of the test matrices corresponding to gray boxes are filled with random values, and those corresponding to white boxes are filled with zeros. The other test matrices are obtained by shifting these pattern horizontally and vertically.

number of the graph by

$$\chi_{\text{nonunif}} \leq 6^d.$$

*A general set of test matrices for extracting inadmissible blocks.* A similar argument proves that extracting inadmissible blocks of the leaf level can be accomplished using  $3^d$  test matrices. The set of boxes activated by one of the test matrices for a problem in two dimensions is shown in Figure 6. Therefore, the chromatic number of the graph described in subsection 4.1.3 is bounded by

$$\chi_{\text{leaf}} \leq 3^d.$$

**4.1.5. Asymptotic complexity.** Let  $L \sim \log N$  denote the depth of the tree,  $T_{\text{mult}}$  denote the time to apply  $\mathbf{A}$  or  $\mathbf{A}^*$  to a vector, and  $T_{\text{flop}}$  denote the time to execute one floating point operation. There are  $2^{dl}$  boxes belonging to level  $l$  of the tree, and the interaction list of each box consists of up to  $6^d - 3^d$  other boxes, so there are approximately  $(6^d - 3^d)2^{dl}$  admissible blocks associated with level  $l$ . The cost of applying the low-rank approximation of an admissible block associated with level  $l$  to a vector is  $\sim kN/2^{dl}$  operations. Therefore, the cost of applying the level- $l$  truncated matrix  $\mathbf{A}^{(l)}$  (or its transpose) to a vector is

$$T_{A^{(l)}} \sim T_{\text{flop}} \times \sum_{j=0}^l (6^d - 3^d) 2^{dj} k \frac{N}{2^{dj}} \sim T_{\text{flop}} \times (6^d - 3^d) l k N.$$

The cost of compressing the admissible blocks associated with level  $l$  of the tree is

$$T_l \sim (T_{\text{mult}} + T_{A^{(l)}}) \times 2\chi_{\text{nonunif}} k + T_{\text{flop}} \times (6^d - 3^d) 2^{dl} k^2 \frac{N}{2^{dl}},$$

since we require  $\sim \chi_{\text{nonunif}} k$  applications of  $\mathbf{A} - \mathbf{A}^{(l)}$  and its transpose, where  $\chi_{\text{nonunif}}$  denotes the chromatic number of the graph described in [subsection 4.1.2](#), and we require an additional  $\sim k^2 N / 2^{dl}$  operations for each admissible block to compute low-rank approximations.

Finally, summing  $T_l$  over each level gives the total time to construct an  $\mathcal{H}^1$  representation as follows. The cost of extracting inadmissible blocks associated with the leaf level of the tree is omitted as it only contributes a lower order term to the overall cost. We also omit the costs associated with the graph coloring problem since it is only worthwhile for problems that exhibit low-dimensional structure, in which case the costs would be much lower than the worst-case analysis would suggest, and we observe in practice that the cost of graph coloring represents a small portion of the total cost of compression. For problems without low-dimensional structure, one may skip the graph coloring step and instead use the general set of test matrices described in [subsection 4.1.4](#).

$$T_{\text{compress}} \sim T_{\text{mult}} \times 2\chi_{\text{nonunif}} k \log N + T_{\text{flop}} \times (6^d - 3^d) 2\chi_{\text{nonunif}} k^2 N (\log N)^2$$

**4.2. Uniform  $\mathcal{H}^1$  matrix compression.** A uniform  $\mathcal{H}^1$  approximation requires for each box  $\tau$  a column basis matrix  $\mathbf{U}_\tau$  and a row basis matrix  $\mathbf{V}_\tau$  such that

$$\mathbf{A}_{\alpha,\beta} \approx \mathbf{U}_\alpha \mathbf{U}_\alpha^* \mathbf{A}_{\alpha,\beta} \mathbf{V}_\beta \mathbf{V}_\beta^*$$

for all admissible pairs  $(\alpha, \beta)$ . In other words,  $\mathbf{U}_\alpha$  must span the column space of  $\mathbf{A}(I_\alpha, \cup_{\beta \in \mathcal{L}_\alpha^{\text{int}}} I_\beta)$ , the submatrix of interactions between  $\alpha$  and the boxes in its interaction list. Similarly,  $\mathbf{V}_\beta$  must span the row space of  $\mathbf{A}(\cup_{\alpha \in \mathcal{L}_\beta^{\text{int}}} I_\alpha, I_\beta)$ . The algorithms for compressing  $\mathcal{H}^1$  and uniform  $\mathcal{H}^1$  matrices have a two important differences. For a uniform  $\mathcal{H}^1$  matrix, we use [Algorithm 2.2](#), rather than [Algorithm 2.1](#) to compute low-rank approximations. Also, instead of sampling the column space of each admissible block  $\mathbf{A}_{\alpha,\beta}$  separately, we will sample the interactions between each box and all of the boxes in its interaction list together.

We return to the task of compressing the admissible blocks associated with level 3 of the tree as described in [subsection 4.1.2](#). As before, we will sample  $\mathbf{A} - \mathbf{A}^{(2)}$  with a set of test matrices. To sample those interactions for some box  $\alpha$ , we require a test matrix  $\mathbf{\Omega}$  that satisfies the following sampling constraints.

$$(4.6) \quad \begin{aligned} \mathbf{\Omega}(I_\beta, :) &= \mathbf{G}_\beta & \text{for all } \beta \in \mathcal{L}_\alpha^{\text{int}} \\ \mathbf{\Omega}(I_\gamma, :) &= \mathbf{0} & \text{for all } \gamma \in \mathcal{L}_\alpha^{\text{nei}} \end{aligned}$$

If test matrix  $\mathbf{\Omega}$  satisfies the above sampling constraints, then the rows of the product  $\mathbf{A}\mathbf{\Omega} - \mathbf{A}^{(2)}\mathbf{\Omega}$  indexed by  $I_\alpha$  will contain a randomized sample of the column space of  $\mathbf{A}(I_\alpha, \cup_{\beta \in \mathcal{L}_\alpha^{\text{int}}} I_\beta)$ , the submatrix of interactions between  $\alpha$  and the boxes in its interaction list.

We have one set of sampling constraints for each box  $\alpha$ , and we use them to form the constraint incompatibility graph ([Definition 4.1](#)) shown in [Figure 7](#). As in [subsection 4.1.2](#), we compute a vertex coloring of the graph. The coloring of the graph



in [Figure 7](#) specifies test matrices with the following structures.

$$[\Omega_1 \quad \Omega_2 \quad \Omega_3 \quad \Omega_4 \quad \Omega_5] = \begin{bmatrix} \mathbf{0} & \mathbf{0} & \mathbf{G}_8 & \mathbf{G}_8 & * \\ \mathbf{0} & \mathbf{0} & \mathbf{0} & \mathbf{G}_9 & * \\ \mathbf{G}_{10} & \mathbf{0} & \mathbf{0} & \mathbf{0} & \mathbf{G}_{10} \\ \mathbf{G}_{11} & \mathbf{G}_{11} & \mathbf{0} & \mathbf{0} & \mathbf{0} \\ \mathbf{0} & \mathbf{G}_{12} & \mathbf{G}_{12} & \mathbf{0} & \mathbf{0} \\ \mathbf{0} & \mathbf{0} & \mathbf{G}_{13} & \mathbf{G}_{13} & \mathbf{0} \\ \mathbf{0} & \mathbf{0} & \mathbf{0} & * & \mathbf{G}_{14} \\ \mathbf{G}_{15} & \mathbf{0} & \mathbf{0} & * & \mathbf{G}_{15} \end{bmatrix}$$

We evaluate the samples  $\mathbf{Y}_i = \mathbf{A}\Omega_i - \mathbf{A}^{(2)}\Omega_i$  for each test matrix  $\Omega_i$ , and orthonormalize the relevant blocks of the sample matrices  $\mathbf{Y}_i$  to obtain orthonormal column basis matrix  $\mathbf{U}_\alpha$  for each box  $\alpha$ . That is, if  $\Omega_i$  is the test matrix satisfying the sampling constraints of box  $\alpha$ , then

$$\mathbf{Y}_i(I_\alpha, :) = \sum_{\beta \in \mathcal{L}_\alpha^{\text{int}}} \mathbf{A}_{\alpha, \beta} \mathbf{G}_\beta,$$

so we compute

$$\mathbf{U}_\alpha = \text{qr}(\mathbf{Y}_i(I_\alpha, :)).$$

For the second stage of compression using [Algorithm 2.2](#), we must compute  $\mathbf{A}_{\alpha, \beta}^* \mathbf{U}_\alpha$  for each admissible block  $\mathbf{A}_{\alpha, \beta}$ . To do so, we use the procedure for sampling an  $\mathcal{H}^1$  matrix with non-uniform basis matrices ([subsection 4.1.2](#)), but rather than filling blocks of the test matrices with random values, we fill them with appropriately chosen uniform basis matrices. With that modification, we have the following sampling constraints for each admissible pair  $(\alpha, \beta)$ .

$$\begin{aligned} \Psi(I_\beta, :) &= \mathbf{U}_\beta \\ \Psi(I_\gamma, :) &= \mathbf{0} \quad \text{for all } \gamma \in \mathcal{L}_\alpha^{\text{nei}} \cup \mathcal{L}_\alpha^{\text{int}} \setminus \{\beta\} \end{aligned}$$

We construct a suitable set of test matrices via graph coloring and evaluate the products  $\mathbf{Z}_i = (\mathbf{A} - \mathbf{A}^{(2)})^* \Psi_i$  for each test matrix  $\Psi_i$ . Then for each admissible pair  $(\alpha, \beta)$ , there is some  $\mathbf{Z}_i$  such that  $\mathbf{Z}_i(I_\alpha, :) = \mathbf{A}_{\alpha, \beta}^* \mathbf{U}_\beta$ . With those results, we compute the uniform basis matrices  $\mathbf{V}_\alpha$  and the matrices  $\mathbf{B}_{\alpha, \beta}$  as follows.

$$\begin{aligned} \mathbf{V}_\beta &= \text{qr} \left( \sum_{\alpha \in \mathcal{L}_\beta^{\text{int}}} \mathbf{Z}_i(I_\alpha, :) \right) = \text{qr} \left( \sum_{\alpha \in \mathcal{L}_\beta^{\text{int}}} \mathbf{A}_{\alpha, \beta}^* \mathbf{U}_\alpha \right) \\ \mathbf{B}_{\alpha, \beta} &= \mathbf{Z}_i(I_\alpha, :)^* \mathbf{V}_\beta = (\mathbf{A}_{\alpha, \beta}^* \mathbf{U}_\alpha)^* \mathbf{V}_\beta \end{aligned}$$

*Remark 4.2.* An alternative approach for uniform  $\mathcal{H}^1$  compression [\[16\]](#) is obtained by adding a uniformization step to the  $\mathcal{H}^1$  compression algorithm. With that approach, one first computes low-rank approximations  $\mathbf{A}_{\alpha, \beta} = \mathbf{U}_{\alpha, \beta} \mathbf{B}_{\alpha, \beta} \mathbf{V}_{\alpha, \beta}^*$  with non-uniform basis matrices. Those low-rank approximations are recompressed to obtain uniform basis matrices, followed by a change of basis.

$$\mathbf{A}_{\alpha, \beta} \approx \mathbf{U}_\alpha (\mathbf{U}_\alpha^* \mathbf{U}_{\alpha, \beta} \mathbf{B}_{\alpha, \beta} \mathbf{V}_{\alpha, \beta}^* \mathbf{V}_\beta) \mathbf{V}_\beta^*$$

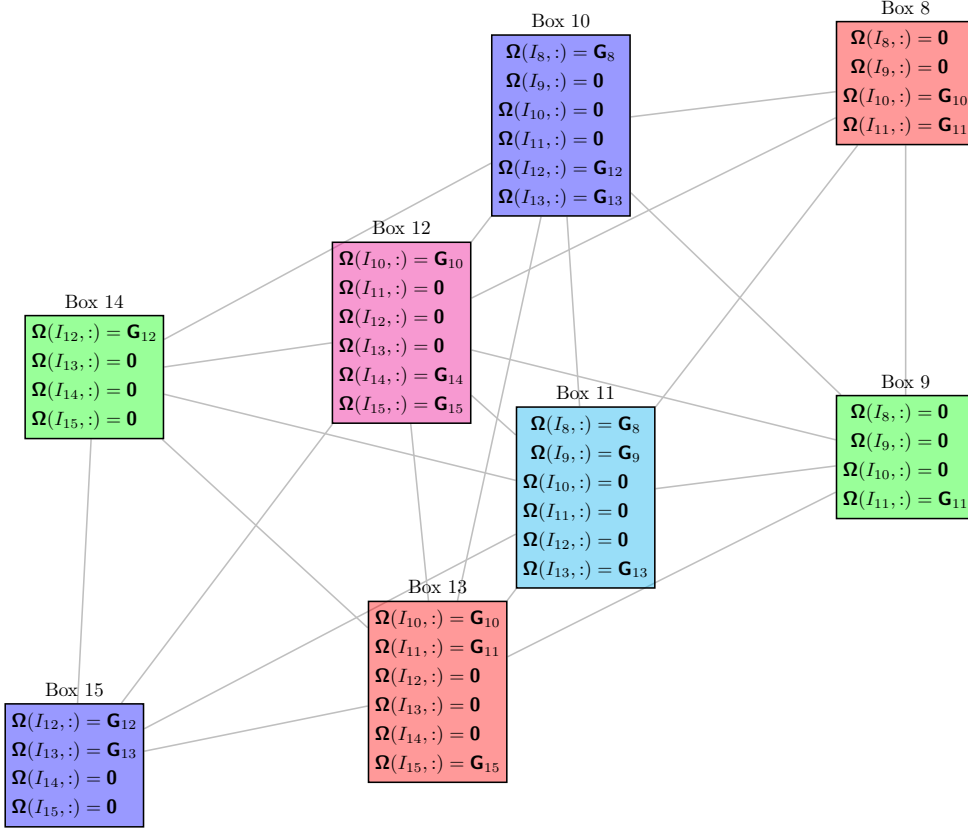


Fig. 7: The constraint incompatibility graph corresponding to the 8 boxes on level 3 of the matrix shown in Figure 3 along with the constraints (4.6) associated with uniform sampling.

One disadvantage of that approach is that  $\mathbf{U}_\alpha$  and  $\mathbf{V}_\alpha$  are based on samples of the factorizations  $\mathbf{U}_{\alpha,\beta} \mathbf{B}_{\alpha,\beta} \mathbf{V}_{\alpha,\beta}^*$ , which may only be approximate, rather than direct samples of the blocks  $\mathbf{A}_{\alpha,\beta}$  themselves, potentially resulting in lower accuracy. Another difference is that the procedure for sampling a uniform  $\mathcal{H}^1$  matrix presented in this section requires fewer matrix-vector products than the procedure for sampling an  $\mathcal{H}^1$  matrix, as described in subsections 4.1.4 and 4.2.1.

**4.2.1. General patterns in the test matrices for uniform  $\mathcal{H}^1$  compression.** As in subsection 4.1.4, we describe a general set of test matrices that is applicable to finer and higher-dimensional grids. To sample the interactions of box  $\alpha$  for a problem in 2 dimensions, the blocks of the test matrix corresponding to the boxes in  $\mathcal{L}_\alpha^{\text{nei}}$  must be filled with zeros, and the blocks corresponding to the boxes in  $\mathcal{L}_\alpha^{\text{int}}$  must be filled with random values (4.6). The pattern of activated boxes for one test matrix is shown in Figure 8. The complete set of 25 test matrices is obtained by shifting the pattern horizontally and vertically. The pattern generalizes to higher-dimensional problems, requiring at most  $5^d$  test matrices to carry out the first stage of uniform

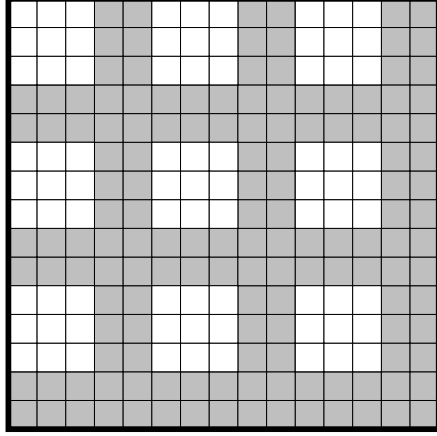


Fig. 8: A pattern representing one test matrix for the first stage of uniform  $\mathcal{H}^1$  sampling for a problem in 2 dimensions. Blocks of the test matrix corresponding to gray boxes are filled with random values, and those corresponding to white boxes are filled with zeros. The other test matrices are obtained by shifting this pattern horizontally and vertically.

$\mathcal{H}^1$  sampling for a problem in  $d$  dimensions. Therefore, we establish the upper bound

$$\chi_{\text{unif}} \leq 5^d.$$

**4.3.  $\mathcal{H}^2$  matrix compression.** To obtain an algorithm for computing an  $\mathcal{H}^2$  representation, we apply two modifications to the algorithm for computing a uniform  $\mathcal{H}^1$  representation. First, we enrich the basis matrices of each box so that they span the relevant parts of the basis matrices of its parent. Specifically, if box  $\tau$  is the parent of box  $\alpha$ , then when computing the basis matrix  $\mathbf{U}_\alpha$ , we augment  $\mathbf{Y}_i(I_\alpha, :)$ , the sample of  $\mathbf{A}(I_\alpha, \cup_{\beta \in \mathcal{L}_\alpha^{\text{int}}} I_\beta)$ , with  $\mathbf{U}_\tau(I_\alpha, :)\boldsymbol{\Sigma}_\tau^{\text{in}}\mathbf{G}_k$ , a sample of  $\mathbf{A}(I_\alpha, (\cup_{\beta \in \mathcal{L}_\tau^{\text{nei}}} I_\beta)^c)$ , where  $\mathbf{G}_k$  is a  $k$ -by- $k$  Gaussian random matrix.

$$\begin{aligned} \mathbf{Y}_i(I_\alpha, :) &= \sum_{\beta \in \mathcal{L}_\alpha^{\text{int}}} \mathbf{A}_{\alpha, \beta} \mathbf{G}_\beta \\ [\mathbf{U}_\alpha, \boldsymbol{\Sigma}_\alpha^{\text{in}}, \sim] &= \text{svd} \left( \mathbf{Y}_i(I_\alpha, :) + \mathbf{U}_\tau \boldsymbol{\Sigma}_\tau^{\text{in}} \mathbf{G}_k \right) \end{aligned}$$

We use a similarly augmented sample when computing  $\mathbf{V}_\alpha$ .

$$[\mathbf{V}_\alpha, \boldsymbol{\Sigma}_\alpha^{\text{out}}, \sim] = \text{svd} \left( \sum_{\beta \in \mathcal{L}_\alpha^{\text{int}}} \mathbf{A}_{\beta, \alpha}^* \mathbf{U}_\beta + \mathbf{V}_\tau \boldsymbol{\Sigma}_\tau^{\text{out}} \mathbf{G}_k \right)$$

Second, after we have computed long basis matrices of its children, we compute the short basis matrix  $\mathbf{U}_\tau$  by solving (3.1), and then we can discard  $\mathbf{U}_\tau$ . Similarly, we compute  $\mathbf{V}_\tau$  and discard  $\mathbf{V}_\tau$ . The process of compressing uniform  $\mathcal{H}^1$  and  $\mathcal{H}^2$  matrices are summarized in Algorithm 4.2. The algorithm for applying a level-truncated approximation of an  $\mathcal{H}^2$  matrix to a vector is given in Algorithm 4.3.

---

**Algorithm 4.2** Randomized compression of a uniform  $\mathcal{H}^1$  or  $\mathcal{H}^2$  matrix

---

**for** level  $l \in [2, \dots, L]$  **do**

    Compute randomized samples of  $\mathbf{A} - \mathbf{A}^{(l)}$

    Construct structured random test matrices  $\{\boldsymbol{\Omega}_i\}$  of size  $N \times (k + p)$  as in [subsection 4.2](#) or [subsection 4.2.1](#)

**for all**  $\boldsymbol{\Omega}_i$  **do**

        Multiply  $\mathbf{Y}_i = \mathbf{A}\boldsymbol{\Omega}_i - \mathbf{A}^{(l)}\boldsymbol{\Omega}_i$

    Compute uniform orthonormal basis matrices  $\mathbf{U}_\alpha$

**for all** boxes  $\alpha$  in level  $l$  **do**

        Identify  $\mathbf{Y}_i$  that contains a sample of  $\mathbf{A}(I_\alpha, \cup_{\beta \in \mathcal{L}_\alpha^{\text{int}}} I_\beta)$  in  $\mathbf{Y}_i(I_\alpha, :)$

**if**  $\mathbf{A}$  has uniform  $\mathcal{H}^1$  structure **then**

            Compute an SVD of the sample:  $[\mathbf{U}_\alpha, \boldsymbol{\Sigma}_\alpha^{\text{in}}, \sim] = \text{svd}(\mathbf{Y}_i(I_\alpha, :), k)$

**else if**  $\mathbf{A}$  has  $\mathcal{H}^2$  structure **then**

            Compute an SVD of the augmented sample:  $[\mathbf{U}_\alpha, \boldsymbol{\Sigma}_\alpha^{\text{in}}, \sim] = \text{svd}(\mathbf{Y}_i(I_\alpha, :)$   
 $) + \mathbf{U}_\tau \boldsymbol{\Sigma}_\tau^{\text{in}} \mathbf{G}_k, k)$

    Compute randomized samples of  $\mathbf{A}^* - \mathbf{A}^{(l)*}$

    Construct structured random test matrices  $\{\boldsymbol{\Psi}_i\}$  of size  $N \times (k + p)$  as in [subsection 4.1.2](#) or [subsection 4.1.4](#)

**for all**  $\boldsymbol{\Psi}_i$  **do**

        Multiply  $\mathbf{Z}_i = \mathbf{A}^* \boldsymbol{\Psi}_i - \mathbf{A}^{(l)*} \boldsymbol{\Psi}_i$

    Compute uniform orthonormal basis matrices  $\mathbf{V}_\beta$

**for all** boxes  $\beta$  in level  $l$  **do**

        Identify  $\mathbf{Z}_i$  that contains  $\mathbf{A}_{\alpha, \beta}^* \mathbf{U}_\alpha$  in  $\mathbf{Z}_i(I_\beta, :)$  for  $\alpha \in \mathcal{L}_\beta^{\text{int}}$

**if**  $\mathbf{A}$  has uniform  $\mathcal{H}^1$  structure **then**

            Compute an SVD of the sample:  $[\mathbf{V}_\beta, \boldsymbol{\Sigma}_\beta^{\text{out}}, \sim] = \text{svd}(\sum_{\alpha \in \mathcal{L}_\beta^{\text{int}}} \mathbf{Z}_i, k)$

**else if**  $\mathbf{A}$  has  $\mathcal{H}^2$  structure **then**

            Compute an SVD of the augmented sample:  
 $[\mathbf{V}_\beta, \boldsymbol{\Sigma}_\beta^{\text{out}}, \sim] = \text{svd}(\mathbf{V}_\tau \boldsymbol{\Sigma}_\tau^{\text{out}} \mathbf{G}_k + \sum_{\alpha \in \mathcal{L}_\beta^{\text{int}}} \mathbf{Z}_{\alpha, \beta}(I_\beta, :), k)$

    Compute  $\mathbf{B}_{\alpha, \beta}$

**for all** interacting pairs  $\alpha, \beta$  in level  $l$  **do**

        Identify  $\mathbf{Z}_i$  that contains  $\mathbf{A}_{\alpha, \beta}^* \mathbf{U}_\alpha$  in  $\mathbf{Z}_i(I_\beta, :)$  for  $\alpha \in \mathcal{L}_\beta^{\text{int}}$

$\mathbf{B}_{\alpha, \beta} = \mathbf{Z}_i^*(I_\beta, :)\mathbf{V}_\beta$

    Nest the basis matrices

**if**  $\mathbf{A}$  has  $\mathcal{H}^2$  structure **then**

**for all** boxes  $\alpha$  in level  $l$  **do**

            Compute  $\mathbf{U}_\alpha, \mathbf{V}_\alpha$  using (3.1)

            Discard  $\mathbf{U}_\alpha, \mathbf{V}_\alpha$

---

Extract the inadmissible blocks of level  $L$  in the same way as in [Algorithm 4.1](#)

---

---

**Algorithm 4.3** Applying an  $\mathcal{H}^2$  level-truncated approximation  $\mathbf{A}^{(l)}$  to vector  $\mathbf{q}$

---

*Build outgoing expansions in level  $l$ .*

**for all** boxes  $\tau$  in level  $l$  **do**

$$\hat{\mathbf{q}}_\tau = \mathbf{V}_\tau^* \mathbf{q}(I_\tau)$$

*Build outgoing expansions for levels coarser than  $l$  (upward pass).*

**for all** levels  $i \in [l-1, \dots, 2]$  **do**

**for all** boxes  $\tau$  in level  $i$  **do**

**for all** children  $\alpha$  of  $\tau$  **do**

$$\hat{\mathbf{q}}_\tau(I_\alpha, \cdot) = \mathbf{V}_\tau^*(I_\alpha, \cdot) \hat{\mathbf{q}}_\alpha$$

*Build incoming expansions for boxes in level 2.*

**for all** boxes  $\alpha$  in level 2 **do**

$$\hat{\mathbf{u}}_\alpha = \sum_{\beta \in \mathcal{L}_\alpha^{\text{int}}} \mathbf{B}_{\alpha, \beta} \hat{\mathbf{q}}_\beta$$

*Build incoming expansions for levels finer than 2 (downward pass).*

**for all** levels  $i \in [3, \dots, l-1]$  **do**

**for all** boxes  $\alpha$  in level  $i$  **do**

Let  $\tau$  be the parent of  $\alpha$

$$\hat{\mathbf{u}}_\alpha = \sum_{\beta \in \mathcal{L}_\alpha^{\text{int}}} \mathbf{B}_{\alpha, \beta} \hat{\mathbf{q}}_\beta + \mathbf{U}_\tau(I_\alpha, \cdot) \hat{\mathbf{u}}_\tau$$

*Build incoming expansions for level  $l$ .*

**for all** boxes  $\alpha$  in level  $l$  **do**

$$\mathbf{u}(I_\alpha) = \mathbf{U}_\tau \hat{\mathbf{u}}_\tau + \sum_{\beta \in \mathcal{L}_\alpha^{\text{nei}}} \mathbf{A}(I_\alpha, I_\beta) \mathbf{q}(I_\beta)$$


---

**4.3.1. Asymptotic complexity.** The asymptotic complexity of the  $\mathcal{H}^2$  algorithm is similar to that of the  $\mathcal{H}^1$  algorithm. Since we are now using uniform basis matrices, the cost of applying  $T_{A^{(l)}}$  is lower.

$$\begin{aligned} T_{A^{(l)}} &\sim T_{\text{flop}} \times \left( 2^{dl} k \frac{N}{2^{dl}} + \sum_{j=0}^l (6^d - 3^d) k^2 2^{dj} \right) \\ &\sim T_{\text{flop}} \times (kN + (6^d - 3^d) k^2 2^{dl}) \end{aligned}$$

The number of matrix-vector products to carry out sampling for uniform basis matrices is also lower.

$$T_l \sim (T_{\text{mult}} + T_{A^{(l)}}) \times (\chi_{\text{unif}} + \chi_{\text{nonunif}}) k + T_{\text{flop}} \times (6^d - 3^d) 2^{dl} k^2 \frac{N}{2^{dl}},$$

Summing  $T_l$  over each level, we find that the number of floating point operations is lower than that of [subsection 4.1.5](#) by a factor of  $\mathcal{O}(\log N)$ . As in [subsection 4.1.5](#), we omit the costs associated with graph coloring.

$$\begin{aligned} T_{\text{compress}} &\sim T_{\text{mult}} \times (\chi_{\text{unif}} + \chi_{\text{nonunif}}) k \log N \\ &\quad + T_{\text{flop}} \times k^2 N \left( (\chi_{\text{unif}} + \chi_{\text{nonunif}} + 6^d - 3^d) \log N \right. \\ &\quad \left. + (6^d - 3^d) (\chi_{\text{unif}} + \chi_{\text{nonunif}}) \right) \end{aligned}$$

**5. Numerical experiments.** In this section, we present a selection of numerical results. The experiment in [subsection 5.1](#) demonstrates the ability of the graph coloring approach to exploit low-dimensional structure. In [subsections 5.2 to 5.5](#), we report the following quantities for a number of test problems and rank structure formats: (1) the time to compress the operator, (2) the time to apply the compressed representation to a vector, (3) the relative accuracy of the compressed representation, and (4) the storage requirements of the compressed representation measured as the number of values per degree of freedom. For compression time, we report both the total time taken for compression as well as the “net time,” which does not include the time spent by the black-box multiplication routine. The algorithms for compressing matrices and applying compressed representations are written in Python, and the black-box multiplication routines are written in MATLAB. The experiments were carried out on a workstation with two Intel Xeon Gold 6254 processors with 18 cores each and 754GB of memory.

The matrices are compressed with the  $\mathcal{H}^1$ , uniform  $\mathcal{H}^1$ , and  $\mathcal{H}^2$  formats. For the uniform  $\mathcal{H}^1$  format, we take two approaches: the “ $\mathcal{H}^1$  + unif.” approach uses the  $\mathcal{H}^1$  sampling procedure followed by a uniformization step (based on [\[16\]](#)), and the “unif.  $\mathcal{H}^1$ ” approach uses the technique described in [subsection 4.2](#), which uses a different sampling procedure to sample entire interaction lists and avoids the uniformization step.

We measure the accuracy of the compressed matrices using the relative error

$$\frac{\|\tilde{\mathbf{A}} - \mathbf{A}\|}{\|\mathbf{A}\|}$$

computed via 20 iterations of the power method. We also report the maximum leaf node size  $m$  and the number  $r$  of random vectors per test matrix, which are inputs to the compression algorithm.

**5.1. Exploiting low-dimensional structure.** A major advantage of the graph coloring approach is that it tailors the test matrices to the problem at hand, exploiting low-dimensional structure to minimize the number of matrix-vector products. In [subsections 4.1 to 4.3](#), we establish upper bounds on the chromatic numbers of the graphs in terms of the dimension  $d$  of the computational domain. However, if the geometry of the points exhibits lower-dimensional structure (e.g., a discretization of a surface in three-dimensional space, a machine learning dataset consisting of observations belonging to a high-dimensional feature space), the chromatic numbers may be much lower.

To demonstrate this effect, we color the graphs that arise from sampling one level of admissible blocks of an  $\mathcal{H}^1$  matrix based on a uniform grid along a randomly oriented line through  $[0, 1]^d$  over a range of dimensions  $d$ . We perturb the data by adding Gaussian noise to the coordinates of the points in order to simulate geometries that are not perfectly one-dimensional. With zero noise, the points lie exactly on a line. As more and more noise is added, the effective dimensionality of the data increases from one to the full ambient dimension. The results reported in [Figure 9](#) demonstrate that the number of colors increase modestly in the presence of low-dimensional structure and exponentially in the absence of low-dimensional structure.

**5.2. Boundary integral equation.** We consider a matrix arising from the discretization of the Boundary Integral Equation (BIE)

$$(5.1) \quad \frac{1}{2}q(x) + \int_{\Gamma} \frac{(x-y) \cdot n(y)}{4\pi|x-y|^2} q(y) ds(y) = f(x), \quad x \in \Gamma,$$

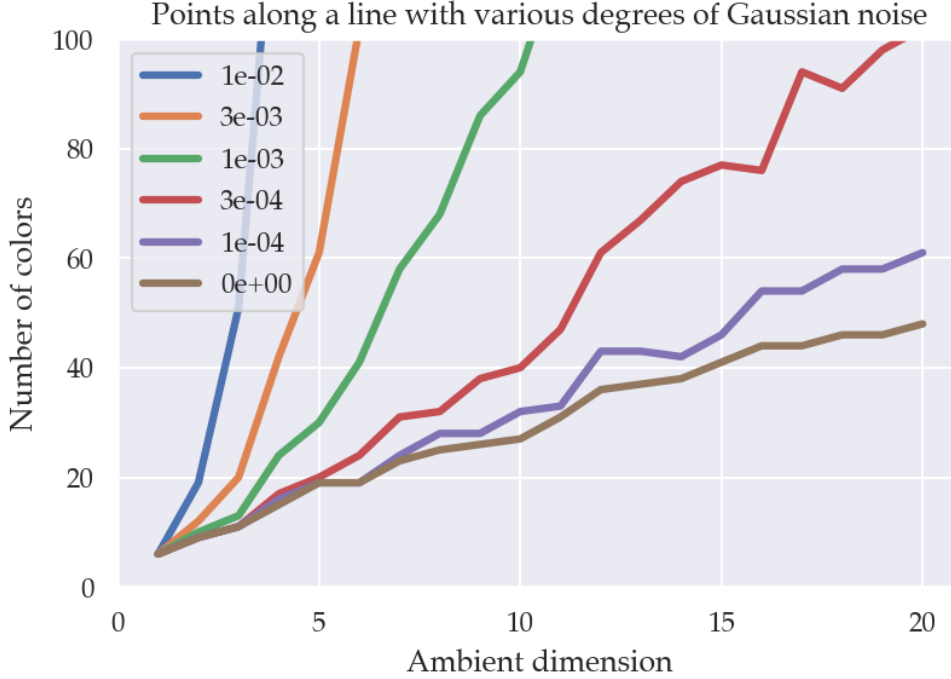


Fig. 9: Number of colors for the incompatibility graphs that arise from sampling one level of admissible blocks of an  $\mathcal{H}^1$  matrix based on a uniform grid along a randomly oriented line through  $[0, 1]^d$  with added perturbation over a range of dimensions  $d$ .

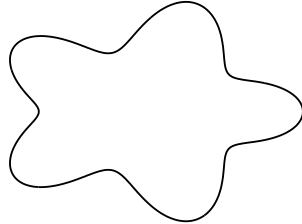


Fig. 10: Contour  $\Gamma$  on which the BIE (5.1) is defined.

where  $\Gamma$  is the simple closed contour in the plane shown in Figure 10, and where  $n(y)$  is the outwards pointing unit normal of  $\Gamma$  at  $y$ . The BIE (5.1) is a standard integral equation formulation of the Laplace equation with boundary condition  $f$  on the domain interior to  $\Gamma$ . The BIE (5.1) is discretized using the Nyström method on  $N$  equispaced points on  $\Gamma$ , with the Trapezoidal rule as the quadrature (since the kernel in (5.1) is smooth, the Trapezoidal rule has exponential convergence).

The fast matrix-vector multiplication is in this case furnished by the recursive skeletonization (RS) procedure of [17]. To avoid spurious effects due to the rank structure inherent in RS, we compute the matrix-vector products at close to double precision accuracy, and with an entirely uncorrelated tree structure.

Results are given in [Figure 13](#).

*Remark 5.1.* The problem under consideration here is artificial in the sense that there is no actual need to use more than a couple of hundred points to resolve (5.1) numerically to double precision accuracy. It is included merely to illustrate the asymptotic scaling of the proposed method.

**5.3. Operator multiplication.** We next investigate how the proposed technique performs on a matrix matrix multiplication problem. Specifically, we determine the Neumann-to-Dirichlet operator  $T$  for the contour shown in [Figure 10](#) using the well known formula

$$T = S \left( \frac{1}{2}I + D^* \right)^{-1},$$

where  $S$  is the single layer operator  $[Sq](x) = \int_{\Gamma} -\frac{1}{2\pi} \log|x-y| q(y) ds(y)$ , and where  $D^*$  is the adjoint of the double-layer operator  $[D^*q](x) = \int_{\Gamma} \frac{n(x) \cdot (x-y)}{2\pi|x-y|^2} q(y) ds(y)$ . The operators  $S$  and  $D$  are again discretized using a Nyström method on equispaced points (with sixth order Kapur-Rokhlin [15] corrections to handle the singularity in  $S$ ), resulting in matrices  $\mathbf{S}$  and  $\mathbf{D}$ . The  $\mathbf{S}(0.5\mathbf{I} + \mathbf{D}^*)^{-1}$  is again applied using the recursive skeletonization procedure of [17].

Results are given in [Figure 12](#).

**5.4. Fast multipole method.** We consider a kernel matrix representing  $N$ -body Laplace interactions in three dimensions, where the interaction kernel is defined by

$$\mathcal{K}(x, y) = \sum_{i \neq j} \frac{c_j}{\|x_i - x_j\|}$$

for a sets of  $N$  points  $\{x_i\}$  and charges  $\{c_i\}$ . To simulate a problem with low-dimensional structure, we distribute the points uniformly at random on the surface of the unit sphere. We use an implementation of the fast multipole method included in the Flatiron Institute Fast Multipole Libraries [2] to efficiently apply the matrix to vectors. Results are given in [Figure 14](#).

**5.5. Frontal matrices in nested dissection.** Our next example is a simple model problem that illustrates the behavior of the proposed method in the context of sparse direct solvers. The idea here is to use rank structure to compress the increasingly large Schur complements that arise in the LU factorization of a sparse matrix arising from the finite element or finite difference discretization of an elliptic PDE, cf. [21, Ch. 21]. As a model problem, we consider an  $N \times N$  matrix  $\mathbf{C}$  that encodes the stiffness matrix for the standard five-point stencil finite difference approximation to the Poisson equation on a rectangle. We use a grid with  $N \times 51$  nodes. We partition the grid into three sets  $\{1, 2, 3\}$ , as shown in [Figure 11](#), and then tessellate  $\mathbf{C}$  accordingly,

$$\mathbf{C} = \begin{bmatrix} \mathbf{C}_{11} & \mathbf{0} & \mathbf{C}_{13} \\ \mathbf{0} & \mathbf{C}_{22} & \mathbf{C}_{23} \\ \mathbf{C}_{31} & \mathbf{C}_{32} & \mathbf{C}_{33} \end{bmatrix}.$$

The matrix we seek to compress is the Schur complement

$$\mathbf{A} = \mathbf{C}_{33} - \mathbf{C}_{31}\mathbf{C}_{11}^{-1}\mathbf{C}_{31} - \mathbf{C}_{32}\mathbf{C}_{22}^{-1}\mathbf{C}_{23}.$$

In our example, we apply  $\mathbf{A}$  to vector by calling standard sparse direct solvers for the left and the right subdomains, respectively.

Results are given in [Figure 15](#).



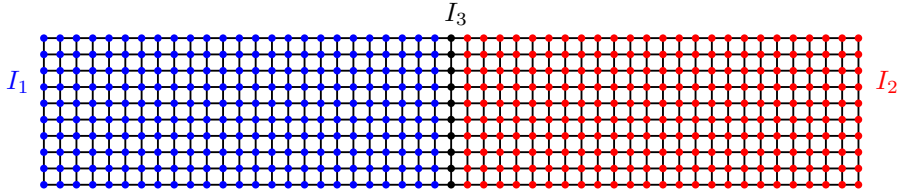


Fig. 11: An example of the grid in the sparse LU example described in Section 5.5. There are  $N \times n$  points in the grid, shown for  $N = 10, n = 51$ .

### 5.6. Summary of observations.

- The results demonstrate quasilinear scaling of computation time for compressing the operators and for applying the compressed representations to vectors.
- The unif.  $\mathcal{H}^1$  compression scheme consistently outperforms the  $\mathcal{H}^1 + \text{unif.}$  scheme. The advantage appears not only in shorter compression times, but also in higher accuracy and lower storage requirements.
- The approximations achieve high accuracy in every case, with the exception of the FMM, for which the accuracy is on par with the accuracy of the operator.
- The storage costs, reported as number of floating point numbers per degree of freedom, remains roughly constant for the  $\mathcal{H}^2$  format, and grows logarithmically for the other formats.
- In every case, the majority of the compression time is spent in the black-box matrix-vector multiplication routines, highlighting the importance of minimizing the number of matrix-vector products.

**6. Conclusions.** This paper presents algorithms for randomized compression of rank-structured matrices. The algorithms only access the matrix via black-box matrix-vector multiplication routines. We formulate a graph coloring problem to design sets of test matrices that are tailored to the given matrix and to minimize the number of matrix-vector multiplications required. Numerical experiments demonstrate that the algorithms are accurate and much more efficient than prior works, particularly when the underlying geometry exhibits low-dimensional structure.

### REFERENCES

- [1] S. AMBIKASARAN AND E. DARVE, *An  $o(n \log n)$  fast direct solver for partial hierarchically semi-separable matrices*, Journal of Scientific Computing, 57 (2013), pp. 477–501.
- [2] T. ASKHAM, Z. GIMBUTAS, L. GREENGARD, L. LU, J. MAGLAND, D. MALHOTRA, M. O’NEIL, M. RACHH, V. ROKHLIN, AND F. VICO, *Flatiron institute fast multipole libraries*. <https://github.com/flatironinstitute/FMM3D>.
- [3] M. BEBENDORF, *Hierarchical matrices*, Springer, 2008.
- [4] S. BÖRM, *Efficient numerical methods for non-local operators*, vol. 14 of EMS Tracts in Mathematics, European Mathematical Society (EMS), Zürich, 2010.  $\mathcal{H}^2$ -matrix compression, algorithms and analysis.
- [5] D. BRÉLAZ, *New methods to color the vertices of a graph*, Communications of the ACM, 22 (1979), pp. 251–256.
- [6] S. CHANDRASEKARAN, P. DEWILDE, M. GU, W. LYONS, AND T. PALS, *A fast solver for hss representations via sparse matrices*, SIAM Journal on Matrix Analysis and Applications, 29 (2007), pp. 67–81.
- [7] S. CHANDRASEKARAN, M. GU, AND T. PALS, *A fast ulv decomposition solver for hierarchically semiseparable representations*, SIAM Journal on Matrix Analysis and Applications, 28

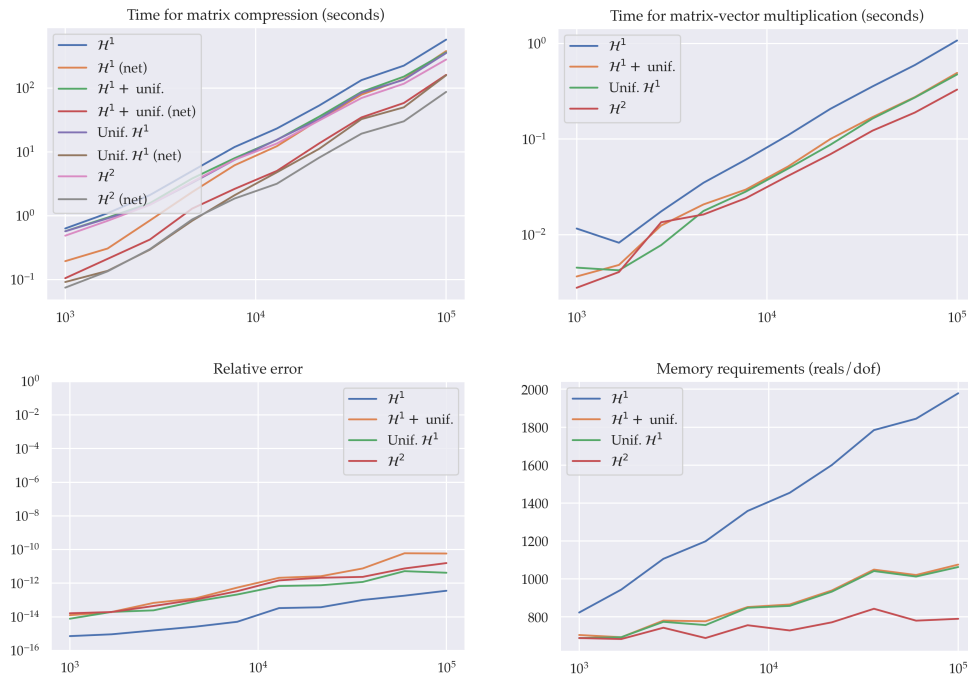


Fig. 12: Results from applying peeling algorithms to the Neumann-to-Dirichlet operator. Here  $r = 20$  and  $m = 200$ .

- (2006), pp. 603–622.
- [8] A. GILLMAN, P. M. YOUNG, AND P.-G. MARTINSSON, *A direct solver with  $o(n)$  complexity for integral equations on one-dimensional domains*, *Frontiers of Mathematics in China*, 7 (2012), pp. 217–247.
  - [9] G. H. GOLUB AND C. F. VAN LOAN, *Matrix computations*, JHU press, 2013.
  - [10] L. GREENGARD AND V. ROKHLIN, *A fast algorithm for particle simulations*, *J. Comp. Phys*, 73 (1987), pp. 325–348.
  - [11] L. GREENGARD AND V. ROKHLIN, *A new version of the fast multipole method for the laplace equation in three dimensions*, *Acta numerica*, 6 (1997), pp. 229–269.
  - [12] W. HACKBUSCH, *A sparse matrix arithmetic based on h-matrices. part i: Introduction to h-matrices*, *Computing*, 62 (1999), pp. 89–108.
  - [13] N. HALKO, P.-G. MARTINSSON, AND J. A. TROPP, *Finding structure with randomness: Probabilistic algorithms for constructing approximate matrix decompositions*, *SIAM review*, 53 (2011), pp. 217–288.
  - [14] K. L. HO AND L. GREENGARD, *A fast direct solver for structured linear systems by recursive skeletonization*, *SIAM Journal on Scientific Computing*, 34 (2012), pp. A2507–A2532.
  - [15] S. KAPUR AND V. ROKHLIN, *High-order corrected trapezoidal quadrature rules for singular functions*, *SIAM Journal on Numerical Analysis*, 34 (1997), pp. 1331–1356.
  - [16] L. LIN, J. LU, AND L. YING, *Fast construction of hierarchical matrix representation from matrix-vector multiplication*, *Journal of Computational Physics*, 230 (2011), pp. 4071–4087.
  - [17] P. MARTINSSON AND V. ROKHLIN, *A fast direct solver for boundary integral equations in two dimensions*, *J. Comp. Phys.*, 205 (2005), pp. 1–23.
  - [18] P.-G. MARTINSSON, *A fast direct solver for a class of elliptic partial differential equations*, *Journal of Scientific Computing*, 38 (2009), pp. 316–330.
  - [19] P.-G. MARTINSSON, *A fast randomized algorithm for computing a hierarchically semiseparable representation of a matrix*, *SIAM Journal on Matrix Analysis and Applications*, 32 (2011), pp. 1251–1274.

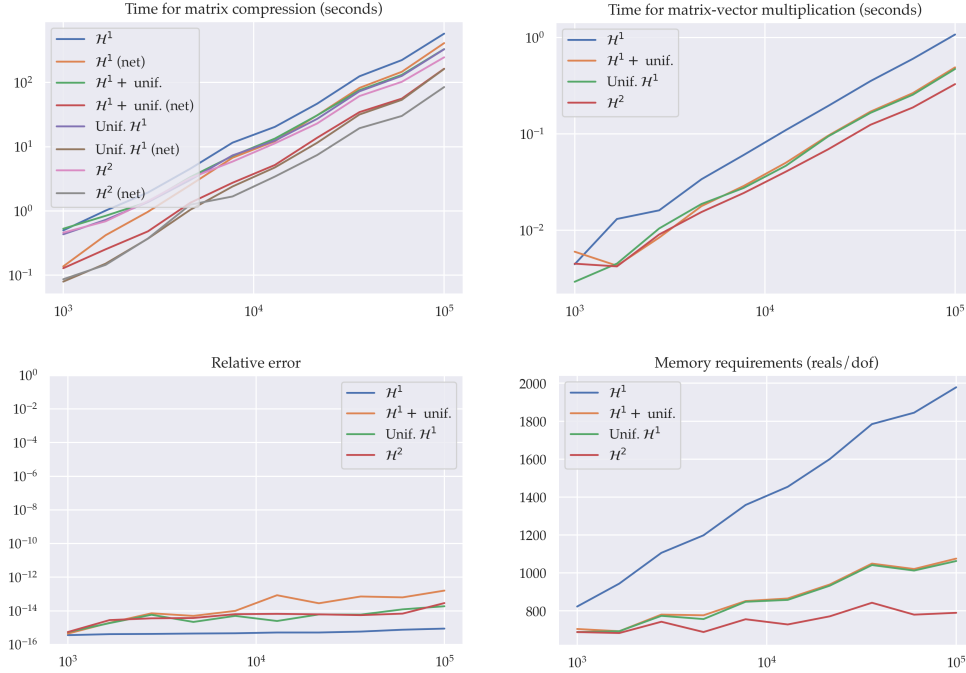


Fig. 13: Results from applying peeling algorithms to a double layer potential on a simple contour in the plane. Here  $r = 20$  and  $m = 200$ .

- [20] P.-G. MARTINSSON, *Compressing rank-structured matrices via randomized sampling*, SIAM Journal on Scientific Computing, 38 (2016), pp. A1959–A1986.
- [21] P.-G. MARTINSSON, *Fast Direct Solvers for Elliptic PDEs*, vol. CB96 of CBMS-NSF conference series, SIAM, 2019, <https://doi.org/10.1137/1.9781611976045>.
- [22] P.-G. MARTINSSON AND J. A. TROPP, *Randomized numerical linear algebra: Foundations and algorithms*, Acta Numerica, 29 (2020), pp. 403–572.
- [23] V. MINDEN, K. L. HO, A. DAMLE, AND L. YING, *A recursive skeletonization factorization based on strong admissibility*, Multiscale Modeling & Simulation, 15 (2017), pp. 768–796.
- [24] J. A. TROPP, A. YURTSEVER, M. UDELL, AND V. CEVHER, *Practical sketching algorithms for low-rank matrix approximation*, SIAM Journal on Matrix Analysis and Applications, 38 (2017), pp. 1454–1485.
- [25] J. XIA, S. CHANDRASEKARAN, M. GU, AND X. S. LI, *Superfast multifrontal method for large structured linear systems of equations*, SIAM Journal on Matrix Analysis and Applications, 31 (2010), pp. 1382–1411.

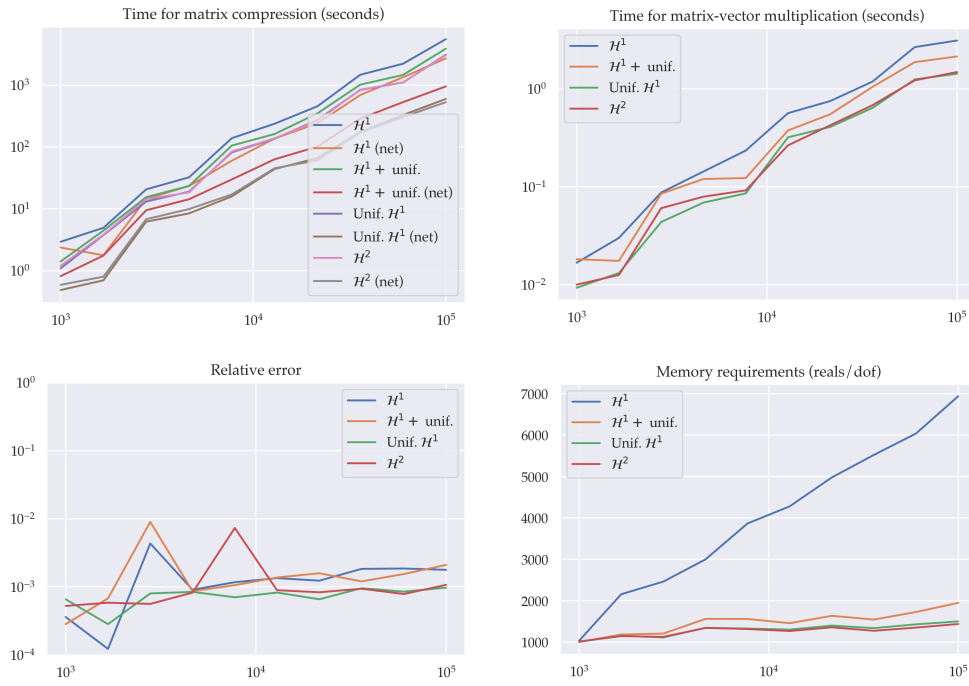


Fig. 14: Results from applying peeling algorithms to the 3D fast multipole method operator. Here  $r = 20$  and  $m = 50$ .

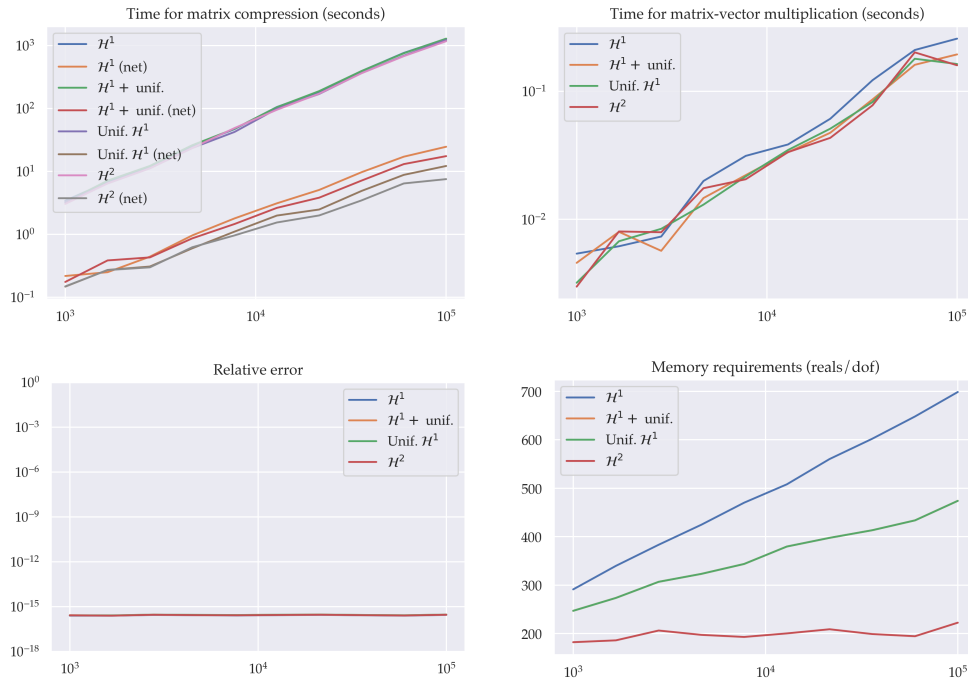


Fig. 15: Results from applying peeling algorithms to frontal matrices in the nested dissection algorithm. Here  $r = 10$  and  $m = 50$ .